HHS Public Access

Author manuscript

Nat Immunol. Author manuscript; available in PMC 2022 February 12.

Published in final edited form as:

Nat Immunol. 2021 September ; 22(9): 1152–1162. doi:10.1038/s41590-021-00987-1.

TCF-1 controls T_{reg} functions that regulate inflammation, CD8 T-cell cytotoxicity, and severity of colon cancer.

Abu Osman[1,2,+], **Bingyu Yan**[3,+], **Ying Li**[4], **Kevin D. Pavelko**[1], **Jasmine Quandt**[2], **Abdulrahman Saadalla**[1], **Mahendra Pal Singh**[1], **Majid Kazemian**[3,5,*], **Fotini Gounari**[2,*], **Khashayarsha Khazaie**[1,*]

[1]Department of Immunology, Mayo Clinic, Rochester, MN

[2]Department of Medicine, Section of Rheumatology, University of Chicago, Chicago, IL

[3]Department of Biochemistry, Purdue University, IN

[4]Division of Biomedical Statistics and Informatics, Mayo Clinic, Rochester, MN.

[5]Department of Computer Science, Purdue University, IN

Abstract

The transcription factor TCF-1 is essential for the development and function of T regulatory (T_{reg}) cells, however its function is poorly understood. Here, we show that TCF-1 primarily suppresses transcription of genes that are co-bound by Foxp3. Single-cell RNA-seq analysis identified effector- and central-memory T_{reg}-cells with differential expression of Klf2 and memory and activation markers. TCF-1 deficiency did not change the core T_{reg} transcriptional signature, but promoted alternative signaling pathways whereby T_{reg}-cells became activated and gained gut-homing and T_H17 characteristics. TCF-1-deficient T_{reg}-cells strongly suppressed T-cell proliferation and cytotoxicity, but were compromised in controlling $CD4^+$ T-cell polarization and inflammation. In mice with polyposis, T_{reg} cell-specific TCF-1 deficiency promoted tumor growth. Consistently, tumor-infiltrating T_{reg} cells of colorectal cancer patients showed lower TCF-1 expression and increased T_H17 expression signatures compared to adjacent normal tissue and circulating T-cells. Thus, T_{reg} cell-specific TCF-1 expression differentially regulates T_H17-mediated inflammation and T-cell cytotoxicity, and can determine colorectal cancer outcome.

Corresponding authors: Khashayarsha Khazaie (Khazaie@mayo.edu), Fotini Gounari (FGounari@UChicago.edu), Majid Kazemian (kazemian@purdue.edu).

[+]These authors contributed equally

[*]These authors jointly supervised this work

Author Contributions

A. O.: Planned and performed experiments, acquired, analyzed and interpreted data, helped with writing of the manuscript.
K. P., J. Q., A. S., M. P. S.: Performed experiments, acquired and analyzed data, prepared figures.
B. Y., Y. L.: Performed scRNA analysis and prepared figures, helped with the interpretation of data and writing of the manuscript.
M. K., F. G., K. K.: Analyzed and interpreted data, prepared figures, wrote manuscript.
K. K.: Conceived the project, designed, and oversaw experiments.

Conflicting Interests

The authors have no conflicting interests.

Introduction

T_{reg}-cells are a heterogenous population of thymic and extrathymic origins with diverse immune suppressive functions. Expression of the lineage-determining transcription factor FOXP3 is essential for maintaining T_{reg} identity [1, 2, 3], but is not sufficient to account for the substantial functional diversity of T_{reg}-cells[4]. In addition to FOXP3, T_{reg}-cells can express other transcription factors that are normally associated with T-helper cell functions, namely RORγT, GATA3, or TBET. More than half of gut-infiltrating T_{reg}-cells in healthy mice express RORγT. RORγT$^+$ T_{reg}-cells are generated from naïve conventional CD4$^+$ T-cells (T_{conv}) upon stimulation by bacterial antigens, and suppress pathobiont induced inflammation in an IL-10 dependent manner [5]. GATA3-expressing T_{reg}-cells express *Ikzf2*/HELIOS and *IL1Rl1*/ST2/IL33-receptor and expand in response to IL-33 [6]. These are mainly of thymic origin, although a subset that potentially originates from T_{conv} cells can convert to RORγT$^+$ T_{reg}-cells[7]. Both RORγT- and GATA3-expressing T_{reg}-cells accumulate in colon tumors, and have T-cell suppressive and tumor-promoting properties [8, 9]. Single-cell RNA-sequencing (scRNAseq) studies of mouse and human cells have identified transcriptionally distinct subpopulations (clusters) of effector-T_{reg} cells (eT_{reg}) and central-memory-T_{reg} cells (cT_{reg}) [7, 10]. However, the molecular underpinning of T_{reg} responses and adaptations at the single cell level to their environment is still poorly understood.

In contrast to healthy mice, expansion of RORγT$^+$ T_{reg}-cells in human colorectal cancer (CRC) coincides with increased colon inflammation [9, 11]. In mouse models of polyposis T_{reg}-specific ablation of RORγT attenuates inflammation and tumor growth [9]. Furthermore, the adoptive transfer of T_{reg}-cells from healthy but not from tumor bearing mice to polyposis prone mice hinders polyposis [12]. We found that T_{reg}-cells in CRC patients and mice with polyposis express elevated levels of β-catenin, which epigenetically programs the cells to become proinflammatory [13, 14]. Our findings were corroborated by an independent report of elevated expression of β-catenin by pro-inflammatory T_{reg}-cells in multiple sclerosis [15]. These findings indicate cancer related changes in T_{reg} functions.

TCF-1 is the T-cell specific DNA binding partner of β-catenin [16]. Germline TCF-1 deficiency induces premature expression of FOXP3 in double-positive thymocytes [17] and expands thymic T_{reg} cells [18], suggesting a role in T_{reg} specification. We and others have shown that TCF-1 and FOXP3 co-bind to overlapping regulatory sites of pro-inflammatory pathway genes [14, 19, 20] and repress the MAF-RORγt-IL-17 axis [14, 21]. Here, we report that in the absence of TCF-1 FOXP3 fails to control these genes and T_{reg}-cells gain promoinflammatory and tumor promoting properties similar to the T_{reg} cells that expand in human CRC and mouse polyposis. Moreover, TCF-1 is downregulated in CRC-tumor-infiltrating T_{reg}-cells. Therefore, TCF-1 differentially controls independent T_{reg} functions that are deregulated in CRC and contribute to tumor growth.

Results

TCF-1 negatively regulates gene expression in T_{reg}-cells

To understand how TCF-1 regulates T_{reg} properties, we generated mice homozygous for the floxed exon4 *Tcf7* [22] and the *Foxp3^{Cre}* alleles [23] (*Foxp3^{Cre}Tcf7$^{fl/fl}$*). FACS analysis

of mesenteric lymph node cells (MLNs) confirmed loss of TCF-1 in T_{reg} but not $CD4^+$ T_{conv} cells (Extended Data Fig.1a,b,c). Bulk RNAseq analysis revealed that deletion of *Tcf7* upregulated 1,090 genes (fold change >1.5 and FDR < 0.001), which included the core T_{reg} signature genes *IL2ra*, *Foxp3*, *Foxo1*, *Tgfb1*, *Lef1*, *Rara*, and *Gata3*, and downregulated 422 genes including *Ctla4*, *Ikzf2*/HELIOS, and *Gzmb* (Fig. 1a). To identify pathways affected, we performed gene set enrichment analysis (GSEA) on all Kegg pathways comparing transcriptomes of T_{reg}-cells from $Foxp3^{Cre}Tcf7^{fl/fl}$ to control $Foxp3^{Cre}$ mice (FDR<0.25; Fig. 1b, Supplementary Table1). The analysis indicated that the TCF-1-deficient T_{reg}-cells preserved the core T_{reg} signature genes (Extended Data Fig.1d), but were enriched in Wnt, MAPK, IL-17, TGFβ, T-cell receptor (TCR) signaling, and T_H17 differentiation pathways (Fig. 1b). The enhanced Wnt signature could result from reversal of TCF-1 inhibition of transcription [16] . The most significantly enriched genes within the leading edge for WNT signaling included *Lef1*, *Lrp5*, *Gsk3b*, *Csnk1e*, *Csnk2a2*, *Ep300*, and *Rac1*; T_H17 differentiation genes included *Tgfb1*, *IL6ra*, *Rara, Stat3*, *Ifngr2*, *Gata3*, and *Tbx21* as well as genes downstream of the TCR; TGFβ signaling genes included *Tgfb1*, *Smad3*, *Smad7*, and *Myc*; TCR signaling genes included *Nfatc1*, *2*, *3*, *Rela*, *Fos*, *Jun*, *PIk3r1*, *Akt1*, *Nfkb1*, *Kras*, and *Plcg1* (Fig. 1c). Earlier identified TCF-1 bound as well as TCF-1 and FOXP3 co-bound genes [14] were highly upregulated in TCF-1-deficient T_{reg}-cells (Fig. 1d), suggesting dominant regulation by TCF-1. Altered gene expression coincided with opening of chromatin at gene regulatory sites, as determined by ChiP-seq, with key examples being *Tgfb1, Stat3, Smad3* and *Il2ra* (Fig. 1e). Collectively, our data show that TCF-1 has a dominant role in its' cooperates with FOXP3 to negatively regulate the activation and functional polarization of T_{reg}-cells.

Using FACS analysis we validated changes in expression of cell surface proteins that mark T-cell activation, CD69, ICOS, PD1, and CD44, and CD62L (Fig. 2a; Extended Data Fig.2a,b,c,h). Loss of TCF-1 increased the T_{reg} to $CD4^+$ T-cell ratios and the frequency as well as absolute numbers of T_{reg}-cells in secondary lymphoid organs (Fig. 2b; Extended Data Fig.2e), but reduced the cell-surface expression of CD25 (Fig. 2b; Extended Data Fig.2f). We confirmed earler reports of activation of T_{conv} cells, marked by changes CD69, ICOS, PD1, and CD44 [20] (Fig. 2c; Extended Data Fig.2a,b,c,d). The TCF-1 deficient T_{reg}-cells expressed higher levels of RORγT, TGFβRI, TGFβRII, and p-SMAD2/3 (Fig. 2d,e; Extended Data Fig.2g), p-STAT5 and p-S6 (a downstream target of mTORC1 that is highly active in T_{reg} cells [24]) (Fig. 2e). Collectively, these results show that TCF-1 deficiency enhances the activation and expression of core T_{reg} signature genes causing the systemic expansion of $ROR\gamma T^+$ T_{reg}-cells.

Molecularly distinct clusters of T_{reg}-cells

To understand how TCF-1 regulates T_{reg} gene expression and heterogeneity, we performed scRNAseq of purified mesenteric lymph node T_{reg}-cells using the 10xGenomics platform (Extended Data Fig.3a) in four types of mice: $Foxp3^{Cre}Tcf7^{fl/fl}$, $Foxp3^{Cre}$, the polyposis prone $APC^{\Delta 468}$, and WT *C57BL/6J (B6)* mice. An unbiased integrative analysis across all four genotypes after regression for potential artifacts using the Seurat platform (see Methods) resulted in 14,487 cells grouped into 10 major subpopulations on UMAP projection (Fig. 3a, Supplementary Table2; see Materials and Methods). These

subpopulations were annotated according to the most salient identified cell markers (Fig. 3b). As expected, the exon-4 deleted *Tcf7* transcripts were still detected across the T_{reg} clusters, although less intensely as compared to the WT *Tcf7* transcript in control *Foxp3Cre* T_{reg}-cells (Extended Data Fig.3b).

We identified two eTreg clusters with activated/effector characteristics, and low expression of Kruppel-like Factor 2 (*Klf2*). These were annotated as Maf and Ikzf2 based on their high expression of the corresponding genes. The Maf cluster had the highest expression of *Rorc*, *Icos, and S100a4* (Fig. 3b,c). cMAF is essential for the generation of RORγT$^+$ T_{reg}-cells and IgA response [25], and is negatively regulated by TCF-1 [21]. Expression of *Rorc*/RORγT by T_{reg}-cells is bacterial dependent [7], suggesting that the Maf cluster represents peripherally induced T_{reg}-cells. The Ikzf2 cluster had the highest expression of *IL7r*, *Rora*, and *Gata3*, and *Klrg1*, and the second highest expression of *Maf* and *Icos* (Fig. 3b,c). Ikzf2 encodes for HELIOS a member of the IKAROS transcription factor family that regulates several T_{reg} suppressive functions [26], and is preferentially but not exclusively expressed by thymus-derived naïve/cT_{reg}-cells [27]. This cluster prominently expressed *Gata3* and its downstream target gene *St2* that encodes a subunit of the IL33-receptor. Thymus-derived T_{reg}-cells, constitute a significant proportion of the GATA3$^+$ *St2* expressing colonic T_{reg}-cells [6], supporting the thymic origin of the Ikzf2 cluster. These two clusters were earlier described as the RORγT$^+$ and the HELIOS$^+$ subsets in mice [7], or as nonlymphoid T-cell like (nLT) T_{reg}-cells in mice and pT_{reg}-cells in humans [10].

The Mif (macrophage migration inhibitory factor) cluster had high expression of *Tgfb1*, *Tnfrsf9*/4-1bb, *Nfkbid*, and *Nr4a1* (Fig. 3b and Extended Data Fig.4). It also expressed *Maf, Icos,* and *Ikzf2* but less than the *Maf* and *Ikzf2* clusters (Fig. 3b,c). Nr4a1/NUR77 is an immediate-early activation gene downstream of the TCR that induces expression of *Tnfrsf9* and *Ikzf2* [28]. High expression of these genes together with *Tgfb1* are characteristics of early TGFβ induced extrathymic T_{reg} cells. Expression of *Hif1a*, a downstream target of β-catenin, was highest in the Mif and Maf clusters, suggesting TCR signaling [29] and a potential link between β-catenin signaling and activation of the Maf/RORγT axis [13, 14].

The remaining clusters expressed naïve/central-memory genes that identify the cT_{reg} [10], and varying levels of *Klf2* (Fig. 3b and Extended Data Fig.4) a nuclear factor that regulates migration of T_{reg}-cells [30]. The Klf2^{++} cluster which had the highest expression of markers of early thymic emigrants (ETE) and homing to secondary lymphoid organs [30], including *Klf2, S1pr1* and *Igfbp4* (Fig. 3b and Extended Data Fig.4). The Klf2$^-$ and Ncoa3 clusters had the lowest expression of these markers, suggesting that they contain more mature cells. The Ncoa3 cluster was outstanding in strong expression of *Ncoa3* (Fig. 3b), a nuclear co-activator and partner of arylhydrocarbone receptor [31], and high expression of *Notch2*. Three other cT_{reg} clusters, the Klf2$^+$, Ifn and Vsp8, expressed intermediate levels of ETE markers, and were together isolated from the main cluster pool (Fig. 3a,b). The Ifn cluster was conspicuous by its expression of multiple interferon response genes including *Stat1*, *Ifit1*, *Ifit3*, *Ifit1bl1*, and *Ifit3b* (Fig. 3b; Extended Data Fig.4). The Vsp8 cluster expressed *Klf2* and *Izumo1r*, markers of cT_{reg}-cells [32], but was unique in strong expression of *Vps8* a subunit of the CORVET complex that is involved in the formation of exosomes [33] (Fig. 3b; Extended Data Fig.4). The Cd63 cluster, had poor expression of *Klf2* and *Izumo1r* (FOLR4),

expressed *Ccl5* and was distant to the other clusters (Fig. 3a,b and Extended Data Fig.4), hence it likely is not a T_{reg} cluster. Overall, expression of *Klf2* and ETE versus activation markers separated the T_{reg} clusters into different stages of maturation.

To better define the T_{reg} clusters, we performed gene ontology pathway analysis on the upregulated genes. The Maf and Ikzf2 clusters highlighted pathways that indicate terminal differentiation, such as lymphocyte activation, immune response, negative regulation of immune system process, positive regulation of cytokine production, and high apoptotic signaling. By contrast, the Mif cluster displayed regulation of response to cytokine stimulus but no other function, consistent an intermediate stage of T_{reg} specification/maturation (Fig. 3d). Since $Klf2^{++}$ and $Klf2^{-}$ were the two largest T_{reg} clusters with the most extreme difference in *Klf2* expression among the cT_{reg}-cells (Fig. 3a,b), we directly compared them using Metascape and identified the 20 most enriched pathways. The $Klf2^{++}$ cluster was enriched for T-cell migration and leukocyte cell-cell adhesion pathways, consistent with being less mature (Fig. 3e), while the $Klf2^{-}$ cluster was enriched for T_H17 cell differentiation, IgA production, and cytokine production (Fig. 3e), indicating a more mature state. Thus, expression of Klf2 appears to correlated with the stage of maturity of T_{reg}-cells.

TCF-1 regulates distinct T_{reg} functions

To better understand the contribution of TCF-1 to T_{reg} identity and function, we made side by side comparison of the scRNAseq data from $Foxp3^{Cre}Tcf7^{fl/fl}$ and control $Foxp3^{Cre}$ mice. Loss of TCF-1 did not alter the spatial distribution or the number of T_{reg} clusters (Fig. 4a, **left panel**), but did suggest a possible increase in the frequency of cells in the Maf and Ikzf2 T_{reg} clusters relative to the less differentiated clusters (Fig. 4a, **right panel**). There were significant changes in the expression of *Maf, Ccr1, and Hsph1* across T_{reg} clusters with the notable common exception of the Ifn cluster (Fig. 4b; Extended Data Fig. 5a,b; Supplementary Table 3). Accordingly, we found across the T_{reg} clusters changes in expression of MAF target genes and T_H17 pathway genes (Extended Data Fig.5c), and corresponding increases in the T_H17 signaling pathway as revealed by GSEA against the Stubbington (Fig. 4c) or the Kegg genesets (Extended Data Fig.5d,e).

The Maf, Ikzf2, $Klf2^{-}$, and Mif clusters had the strongest upregulation of *Ccr9,* a gut homing marker (Fig. 4b; Extended Data Fig.5f). The Maf and Ikzf2 had the strongest increase in expression of *Hsph1* (Fig. 4b), a T_{reg} activation marker [34]. The Maf cluster also had the strongest increase in expression of the gut-associated integrin *Itgae*/CD103/αE-integrin (Fig. 4b), and together with the Ikzf2 cluster the strongest increase in expression of Fibrinogen-like-protein-2 (*Fgl2*) [35], a downstream target of TIGIT (Fig. 4b). All TCF-1-deficient clusters had uniformly increased expression of *Dnaja1*, which encodes a heat shock protein co-chaperone [36] (Fig. 4b), and *Erdr1,* which encodes a bacteria-sensitive secreted apoptotic factor [37] (Extended Data Fig.5g), but downregulated *Igfbp4*, an inhibitor of insulin-like growth factor receptor signalling [38] (Fig. 4b and Extended Data Fig.5h). The Ifn cluster was the only cluster that did not show significant changes with loss of TCF-1 (Fig. 4b and Extended Data Fig.5b). The Vps8 cluster was unique in having high T_H1 as well as T_H17 signatures (Fig. 4c), raising speculation that this cluster may be precursor to

pathogenic T_H17 cells, which co-express T_H1 and T_H17 cytokines [39]. These results highlight enhanced T_{reg} activation, gut homing, and T_H17 polarization with the loss of TCF-1.

Next, we determined how loss of TCF-1 affects the expression of genes that normally bind TCF-1, by integrating earlier generated ChIPseq analysis data [14]. Overall these genes were upregulated with the loss of TCF-1, indicating negative regulation of gene expression by TCF-1; exception were the Ikzf2, Ncoa3, and Ifn clusters that remained unchanged (Fig. 4d,e). Importantly, expression of TCF-1 and FOXP3 co-bound genes also increased upon loss of TCF-1 (Fig. 4f,g). indicating that TCF-1 cooperates with FOXP3 to suppresses gene expression. Collectively these findings are consistent with TCF-1 functioning as a dominant regulator of FOXP3 in suppressing expression of T_{reg} genes involved in T_H17 signaling, gut homing, and bacterial response.

To better understand the inter-cluster relations of T_{reg}-cells, we overlaid RNA velocity vectors on the UMAP projection. RNA velocity uses scRNAseq data of unspliced and spliced mRNAs to predict future states of transcriptionally distinct clusters of cells [40]. Maf and Ikzf2 were identified as terminally differentiated T_{reg} clusters, which derived from less mature clusters . While the Mif cluster exclusively gave rise to the Maf cluster, the $Klf2^-$ and Ncoa3 were immediate precursors to Ikzf2 (Fig. 4h). There was also some indication for interconversion of Ilzf2 to Maf, in agreement with an earlier report that $HELIOS^+$ T_{reg}-cells can be induced to express RORγT [7]. The Ifn, Vps8 and $Klf2^+$ clusters were isolated and less related to the other clusters, encouraging speculations that they may be intermediates to alternative fates, perhap effector T-cells. In total, the velocity analysis revealed stages of T_{reg} specification and maturation, as well as potential differentiation to non-T_{reg}-cells.

Polyposis causes activation and polarization of T_{reg}-cells

We next performed scRNAseq analysis of T_{reg}-cells from the MLNs of WT and polyposis ridden $APC^{\Delta 468}$ mice. Distribution and numbers of T_{reg} clusters were similar to the $Foxp3^{Cre}Tcf7^{fl/fl}$ and $Foxp3^{Cre}$ mice (Extended Data Fig.6a; Supplementary Table4). In both mice, expression of *Tcf7* was lower in the terminally differentiated Maf and Ikzf2 eT_{reg} clusters as compared with the less matured cT_{reg} clusters (Extended Data Fig.6b). Comparison of gene expression between WT and $APC^{\Delta 468}$ T_{reg}-cells revealed upregulation of Socs3, JunD, Lag3, and *Tgfb1* during polyposis (Extended Data Fig.6c,d). SOCS3 regulates IL-23-mediated STAT3 phosphorylation and polarization of $CD4^+$ T-cells to the T_H17 lineage [41]. *JunD*, encodes an AP1 transcription factor that is activated downstream of the TCR [42]. LAG3 mediates immune suppression by T_{reg} cells [43]. Velocity analysis revealed conserved intercluster relations (Extended Data Fig.6e). Collectively, these transcriptional changes are consistent with the activation and T_H17 polarization of T_{reg} cells during polyposis.

TCF-1 regulates T_{reg}-cell suppression of $CD8^+$ T-cells

We next related our molecular data to T_{reg} function. Earlier we and others had reported that T_{reg} suppression of $CD8^+$ T-cell cytotoxicity is TGFβR dependent [44, 45, 46]. Given their activated expression profile, preservation of the core T_{reg} signature, and the enhanced TGFβ signature, we predicted that TCF-1-deficient T_{reg}-cells would efficiently suppress

CD8$^+$ T-cells. To test this, we compared CD8 cytotoxic responses of *Foxp3^{Cre}Tcf7$^{fl/fl}$* and *Foxp3^{Cre}* mice to acute infection with Theiler's murine encephalomyelitis virus (TMEV), using an *in vivo* kill assay. In an earlier study we described an immunodominant virus-specific CD8$^+$ T-cell response to the viral VP2$_{121\text{-}130}$ peptide that peaks on day 7 post infection[47]. We quantified this activity by adoptive transfer of an equal mix of TMEV-VP2$_{121\text{-}130}$ peptide pulsed and unpulsed splenocytes, at the peak of response to viral infection. Lysis of the peptide pulsed cells was significantly less effective in the *Foxp3^{Cre}Tcf7$^{fl/fl}$* than the *Foxp3^{Cre}* mice (~21% versus ~56% converted, p< 0.0001 Student's t-test) and treatment of mice with LY3200882 abrogated this difference (Fig. 5a). Using tetramers we found that infection of *Foxp3^{Cre}* mice triggered a nearly 14-fold expansion of VP2$_{121\text{-}130}$-specific CD8$^+$ T-cells in the spleen, from 0.07% to almost 1% (p=0.004) of total CD8$^+$ T-cells at the peak of response to TMEV. This expansion was reduced in the *Foxp3^{Cre}Tcf7$^{fl/fl}$* mice to the level of baseline uninfected *Foxp3^{Cre}* mice (Fig. 5b). To independently validate this inhibition, we performed *in vitro* proliferation inhibition assays. FACS purified CD4$^+$CD25$^+$YFP$^+$ T$_{reg}$-cells were cocultured with an equal number of naïve CD4$^+$CD25$^-$CD62L^{hi}CD44^{lo} T-cells and then stimulated with allogeneic BALB/c CD11c$^+$ dendritic cells (DC) and αCD3. The TCF-1-deficient T$_{reg}$-cells exhibited stronger suppressive activity than TCF-1-sufficient T$_{reg}$ cells (p<0.05; Student's t-test) (Fig. 5c). Together, our data show that TCF-1 deficiency augments the ability of T$_{reg}$-cells to suppress CD8$^+$ T-cell cytotoxicity and T-cell proliferation.

TCF-1 regulates T$_{reg}$ suppression of inflammation

Inflammation requires CD4$^+$ T-cell help. Therefore we compared TCF-1-deficient and sufficient T$_{reg}$ cells for their ability to suppress polarization of naïve CD4$^+$ T-cells to T$_H$1 or T$_H$17 lineage. For the *in vitro* assays, spleen CD4$^+$ lymphocytes containing both T$_{conv}$ and T$_{reg}$-cells were purified from *Foxp3^{Cre}Tcf7$^{fl/fl}$* and control *Foxp3^{Cre}* mice, stimulated with αCD3 and αCD28 under T$_H$1 or T$_H$17 polarization conditions for four days. The T$_H$1 polarized T-cells from *Foxp3^{Cre}Tcf7$^{fl/fl}$* mice expressed significantly more IFNγ than the T-cells from *Foxp3^{Cre}* mice (~25% versus ~9% converted, p<0.0004) (Fig. 6a). To standardize the CD4$^+$ T-cell to T$_{reg}$ ratios, we repeated the assay using sorted CD4$^+$CD25$^-$CD62L^{hi}CD44^{lo} naïve T-cells from WT CD45.1 mice mixed at equal ratio with CD25$^+$YFP$^+$ T$_{reg}$-cells from *Foxp3^{Cre}Tcf7$^{fl/fl}$* or control *Foxp3^{Cre}* mice. TCF-1-deficient T$_{reg}$-cells were consistently less effective in suppressing CD4$^+$ T-cell polarization to T$_H$1 (Fig. 6b) (~16% versus ~8% converted, p < 0.002). Similarly, the T$_H$17 polarized T-cells from *Foxp3^{Cre}Tcf7$^{fl/fl}$* mice expressed significantly more IL-17A than the T-cells from *Foxp3^{Cre}* mice (Fig. 6c) (~20% versus ~5% converted, p< 0.0003), and this was confirmed when equal numbers of purified T$_{conv}$ and T$_{reg}$-cells were mixed (Fig. 6d) (~11% versus ~5% converted, p < 0.001). Thus, TCF-1 deficiency compromised the ability of T$_{reg}$-cells to suppress pro-inflammatory T$_H$ cell polarization, to T$_H$1 or T$_H$17.

We further validated our findings using well established conditions that elicit T$_H$1 or T$_H$17 immunity *in vivo*. Mice were infected with TMEV and after seven days mononuclear cells isolated from the spleen or MLNs were re-stimulated *ex vivo* with PMA/Ionomycin/ Golgistop to measure intracellular IFNγ. CD4$^+$ and CD8$^+$ T-cells from *Foxp3^{Cre}Tcf7$^{fl/fl}$* mice expressed significantly more IFNγ than cells from *Foxp3^{Cre}* mice (Fig. 6e,f) (CD4:

MLN 6% versus 3%, p <0.04 & spleen 19% versus 12% p<0.001, CD8: MLN 26% versus 14% p<0.003 & spleen 41% versus 24% p<0.001). To measure T_H17 polarization we followed an established protocol [48], injected the mice intraperitoneally (IP) with αCD3 and four days later quantified the expression of IL-17A by $CD4^+$ T-cells in the small bowel by FACS. The *Foxp3*^{Cre}*Tcf7*$^{fl/fl}$ mice generated significantly more IL-17-expressing CD4 T-cells than the control *Foxp3*^{Cre} mice (p< 0.01) (Fig. 6g). Collectively, these findings indicate that TCF-1-deficient T_{reg}-cells are compromised in suppressing T_H1 and T_H17 polarization *in vitro* and *in vivo*.

TCF-1-deficient T_{reg}-cells promote tumor growth

To assess the tumor-promoting properties of TCF-1-deficient T_{reg}-cells, we crossed the polyposis-prone *APC*$^{\Delta 468}$ mice [49] with *Foxp3*^{Cre}*Tcf7*$^{fl/fl}$ or *Foxp3*^{Cre} mice and aged the compound mutant mice to develop polyps. The TCF-1-deficient *APC*$^{\Delta 468}$*Foxp3*^{Cre}*Tcf7*$^{fl/fl}$ mice had significantly more colon polyps than control *APC*$^{\Delta 468}$*Foxp3*^{Cre} mice (12% versus 4% p<0.0001) (Fig. 7a), while tumor load in the small intestine did not change (Fig. 7b). Nuclear β-catenin staining revealed higher incidence of pre-invasive tumors in both the colon (Fig. 7c) and small bowel (Fig. 7d) of the *APC*$^{\Delta 468}$*Foxp3*^{Cre}*Tcf7*$^{fl/fl}$ mice (Fig. 7e), compared with *APC*$^{\Delta 468}$Foxp3^{Cre} mice (Fig. 7f). The *APC*$^{\Delta 468}$*Foxp3*^{Cre}*Tcf7*$^{fl/fl}$ colon tumors had high densities of $Gr1^+$ compared to *APC*$^{\Delta 468}$*Foxp3*^{Cre} mice (116 per FOV versus 62 per FOV ; p< 0.0001) (Fig. 7g,h), as did the small bowel tumors (13.5 per FOV) versus *APC*$^{\Delta 468}$*Foxp3*^{Cre} mice (8.5 per FOV; p< 0.02) (Fig. 7i,j). The increase in $Gr1^+$ cells was also evident in the tumor-distant healthy tissue (colon: 1.2 versus 0.4 per FOV; p<0.009 and small bowel: 2 versus 1 per FOV; p<0.01) (Fig. 7g,h,i,j). Based on these findings we conclude that TCF-1 deficient T_{reg}-cells have enhanced tumor promoting properties, which relates in part to their compromised suppression of inflammation.

TCF-7 is downregulated in T_{reg}-cells of CRC tumors

To determine the clinical relevance of our findings, we reanalyzed publicly available scRNA-seq data from 12 CRC patients [50], focusing on the T_{reg}-cells from paired peripheral blood mononuclear cells (PBMC), tumor, and adjacent normal tissues. Tumor infiltrating T_{reg}-cells had significantly lower expression of *TCF7* compared to adjacent normal tissue and PBMC (Fig. 8a). Moreover, genes that were highly expressed in tumor infiltrating T_{reg}-cells were enriched in Kegg T_H17 differentiation and IL-17 signaling pathways (Fig. 8b,c,d). These findings are consistent with our earlier observations in CRC patients [9, 11, 51]. Furthermore, they establish the relevance of our findings with TCF-1 mice harboring deficient T_{reg}-cells to the immune pathology of CRC.

Discussion

We have provided evidence that TCF-1 differentially controls independent T_{reg} suppressive mechanisms. TCF-1 deficient T_{reg}-cells gained a “split personality” similar to T_{reg}-cells in CRC [52], failing to suppress inflammation but becoming more active in suppressing T-cell proliferation and cytotoxicity. In a mouse model of spontaneous polyposis, these changes fueled tumor growth by promoting inflammation while blocking antigen specific CD8 T-cell responses. We demonstrated the relevance of these findings to CRC in humans by

meta-analysis of publicly available data, which showed that tumor infiltrating T_{reg}-cells had reduced TCF-1 expression and increased of T_H17 and IL-17 signaling.

TCF-1-deficient T_{reg}-cells strongly expressed the core T_{reg} signature genes, along with Wnt, T_H17, MAPK, and TCR signaling. The scRNAseq, identified two eT_{reg} clusters [7], marked by high expression of *cMaf* or *Ikzf2*, and assigned several cT_{reg} clusters to different stages of maturation based their expression of Klf2, ETE, and activation markers as well as their spatial distribution in the UMAP. This classification was confirmed by pathway analysis. Gene expression data strongly suggested peripheral and thymic origins of the Maf and Ikzf2 clusters respectively. Our UMAP superimposed velocity analysis suggested intercluster relations, indicating that the Maf and Ikzf2 eT_{reg} clusters might originate from two cT_{reg} clusters with low *Klf2* expression, namely $Klf2^-$ and Ncoa3, while the Mif cluster exclusively led to the Maf cluster. Among the cT_{reg} clusters, Ifn, Klf2+, and Vps8 were the most isolated, based on velocity analysis, and could represent transitions to effector T-cells.

Changes in gene expression caused by loss of TCF-1 occurred within conserved T_{reg} clusters. Side by side comparison of scRNAseq data from TCF-1 deficient and sufficient T_{reg}-cells revealed changes in activation, T_H17 signaling, and gut homing. Ablation of TCF-1 broadly enhanced expression of genes that are normally bound by TCF-1 and FOXP3 with few exceptions, such as the Ikzf2/HELIOS cluster. Expression of *cMaf,* and T_H17 signaling signature was increased across T_{reg} clusters, again with little change in the Ikzf2/HELIOS cluster. These findings agrees with our earlier finding that in patients with inflammatory bowel disease and dysplasia expression of proinflammatory cytokines (IL-17, IFNγ, TNF α) by T_{reg}-cells is mostly limited to the $ROR\gamma T^+HELIOS^-$ T_{reg}-cells [14].

Using *ex vivo* and *in vivo* assays we demonstrated that TCF-1 deficient T_{reg}-cells strongly suppressed T-cell proliferation and antigen-specific T-cell cytotoxicity of $CD8^+$ T-cells, however, they were compromised in hindering the polarization of $CD4^+$ T-cell to the pro-inflammatory T_H17 or T_H1 lineages and failed to suppress inflammation in polyposis. Notably, pharmacologic inhibition of TGFβR1 signaling blocked the suppression of CD8 cytotoxicity by TCF-1 deficient T_{reg}-cells, in line with active TGFβ signaling in the absence of TCF-1 and the essential role of this pathway in T_{reg} suppression of CD8 T-cells [44, 46]. The combined pro-inflammatory and T-cell suppressive action of TCF-1 deficient T_{reg}-cells increased tumor load and tumor aggression in polyposis, demonstrating relevance to CRC. These findings demonstrate a bifurcation of T_{reg} suppressive activities upon loss of TCF-1, which favors tumor growth.

Polyposis in mice upregulated T_{reg} genes associated with activation, inflammation, and immune suppression, similar to TCF-1 deficient T_{reg}-cells. At the single cell level, TCF-1 expression was lower in the most differentiated relative to the less mature T_{reg} clusters. We found these findings to be relevant to human CRC. Re-analysis of publicly available data [50] showed reduced TCF-1 expression in tumor infiltrating T_{reg}-cells in CRC. These observations are in line with the tumor dependence T_{reg} pro-inflammatory properties in CRC patients and in polyposis mice [9, 11, 51].

FOXP3 participates in regulatory complexes that activate or suppress gene expression to determine T_{reg} identity[53]. TCF-1 substantially overlaps with FOXP3 in its' binding to regulatory elements of genes of responsible for T-cell activation, migration, and T_H17 differentiation, indicating that it cooperates with FOXP3 to determine T_{reg} fate and function [14, 20]. FOXP3 downregulates the expression of TCF-1 [54] and here we show that ablation of TCF-1 results in the upregulation of FOXP3. Importantly, T_{reg}-cells that lack TCF-1 fail to control the expression of pro-inflammatory genes that normally co-bind TCF-1 and FOXP3. We therefore propose that the interplay between TCF-1 and FOXP3 at co-bound gene regulatory elements differentially regulates independent T_{reg} functions. Under normal physiological conditions this could be beneficial and help eradicate infections while avoiding autoimmunity, but in the setting of CRC these properties fuel tumor growth while blocking cancer immune surveillance [13, 14].

Induction of RORγT in T_{reg}-cells is bacterial dependent, but how dysbiosis which is a known characteristic of CRC, alters the function of RORγT$^+$ T_{reg}-cells remains poorly understood. Here we found that expression of *Erdr1*, a gene that encodes a bacterial sensitive secreted apoptotic factor [37], is upregulated in TCF-1 deficient T_{reg}-cells. Future studies are warranted to elucidate how bacteria alter TCF-1 signaling and T_{reg} functions in CRC, and how they can be exploited to help prevent CRC or improve response to therapy .

Methods

Mice

Mouse strains described below were housed and bred at the Mayo Clinic animal facility. *Tcf7*$^{fl/fl}$ (European Mouse Mutant Archive, EMMA) [22] were crossed to *Foxp3*$^{Cre\text{-}YFP}$ mice [23] (designated as *Foxp3*^{Cre} mice) to generate mice with T_{reg}-cell specific deletion of *Tcf7*. *Foxp3*^{Cre} *Tcf7*$^{fl/fl}$ and control *Foxp3*^{Cre} mice were crossed to *APC*$^{\Delta 468}$ mice [49] to generate the polyposis prone compound mutant *APC*$^{\Delta 468}$ *Foxp3*^{Cre} *Tcf7*$^{fl/fl}$ and *APC*$^{\Delta 468}$ *Foxp3*^{Cre} mice. Animal experiments were approved by the Animal Ethics Committee of the institutes responsible for housing the mice. Unless otherwise specified, all experimental procedures were performed on 5.5 month-old laboratory mice.

Viral infections

Mice were infected with Murine Theiler's Encephalomyelitis Virus (TMEV) at day 0. For acute viral infection, 2.5-5.0 × 10^5 plaque-forming units (PFU) was used. Virus was prepared in plain DMEM and injected intraperitoneally (*i.p.*).

In vivo cytotoxicity assay

In vivo CTL assays followed established protocols [44, 55]. Briefly, splenocytes from naive WT CD45.1 background mouse were prepared as single-cell suspensions to 1 × 10^7/ml in Ca/Mg-free Hanks' balanced salt solution (HBSS) (GE Healthcare). The specific target population (half of the cells) was pulsed with 1μM/ml $VP2_{121\text{-}130}$ peptide and the negative control target population (half of the cells) was not pulsed with peptide. Cells were incubated for 60 min at 37 °C, then were washed twice in complete media and brought up in Ca/Mg-free HBSS for labeling with carboxyfluorescein succinimidyl ester (CFSE;

79898 BioLegend). Peptide pulsed cells were incubated with 10 μM CFSE ($CFSE^{hi}$) or non-pulsed with 1 μM CFSE ($CFSE^{lo}$) concentrations for 10 min in a 37 °C water bath, and then quenched by addition of complete media. Cells were washed three times, then viable cells counted and mixed in a 1:1 ratio prior to injection into recipient mice. A total of 15 million cells per 200 μl Ca/Mg-free PBS (Lonza) (at room temperature) were transferred into mice on day 7 post TMEV, by *i.v.* injection into the tail. Recipient mice were euthanized 4 h later, and the harvested mesenteric lymph nodes and splenocytes were analyzed by flow cytometry to determine the percentage of $CFSE^{hi}$ and $CFSE^{lo}$ cells. The percentage of $VP2_{121\text{-}130}$ -specific cytotoxicity was calculated as follows:

$$\% \text{ specific lysis} = 1 - \frac{rnaive}{rinfected} x\,100\,.\; r = \frac{\%\; CFSE^{lo}\; cells}{\%\; CFSE^{hi}\; cells}$$

In some experiments, mice were gavaged twice a day with TGFβR1 inhibitor (LY3200882, Eli Lilly) 105 mg/kg body weight or 1% hydroxyethyl-cellulose (09368; Sigma) as vehicle from the day of infection till day 7 post infection. Then the cytotoxicity was measured as described above.

Dissociation of mesenteric lymph nodes (MLNs) and spleen

A single cell suspension was obtained from MLNs and splenocytes after physical dissociation with a 40 μm mesh (Falcon). Red blood cell lysis on splenocytes was performed using 1 ml of ACK lysis buffer (Lonza) for 1 min on ice and washed in PBS-2% FBS (F8067; Sigma) buffer.

Enzymatic dissociation of small bowel and colon

Tissue was dissociated using the following steps. Fat layers were removed, washed, and opened longitudinally. Tissues were then minced and dissociated in a cocktail solution of 12 mg collagenase IV (LS004188; Worthington), 180 U DNase (D5025; Sigma) and 1.2 mg hyaluronidase (H3506; Sigma) in 20 ml complete RPMI-1640 media with constant stirring for 25 min at 37 °C. Single cell suspensions were then filtered, and supernatants were washed in PBS-2% FBS. Tissues were digested twice. A percoll (P1644; Sigma) gradient was then performed to remove platelets and debris by layering the 44 % percoll cell suspension over 67 % percoll and centrifuging at 400 g for 20 min at 4 °C without brake. The mononuclear cell layer was collected and washed in PBS-2% FBS buffer.

Flow cytometry

Cells were stained with LIVE/DEAD Fixable Blue Stain (dilution: 1/750; L34962; Invitrogen) and antibodies for 30 min at 4 °C. The fluorochrome-conjugated antibodies were as follows: anti-CD4-PerCP/Cyanine5.5 (dilution: 1/300; clone: RM4-5; Cat: 116012) or anti-CD4-AF700 (dilution: 1/200; clone: RM4-5; cat: 116022) or anti-CD4-Brilliant Violet 785 (dilution: 1/300; clone: RM4-5; Cat: 100551), anti-CD25-Brilliant Violet 650 (dilution: 1/200; clone: PC61; cat: 102038), anti-CD44-Brilliant Violet 785 (dilution: 1/500; clone: IM7; cat: 103059), anti-CD278 (ICOS)-PE-Cy7 (dilution: 1/200; clone: C398.4A; cat: 313520), anti-CD279 (PD-1)-Brilliant Violet 421 (dilution: 1/200; clone: 29F.1A12; cat:

135218), anti-CD45.1-PE/Cy7 (dilution: 1/500; clone: A20; cat: 110730) or anti-CD45.1-BV650 (dilution: 1/500; clone: A20; cat: 110735), anti-CD45.2-APC (dilution: 1/500; clone: 104; cat: 109814) (all from BioLegend); anti-CD8a-V500 (dilution: 1/200; clone: 53-6.7; cat: 560776), anti-CD62L-FITC (dilution: 1/200; clone: MEL-14; cat: 553150), anti-CD69-Brilliant Violet 785 (dilution: 1/200; clone: H1.2F3; cat: 564683) (all from BD Biosciences). 50 μl of a 1:50 dilution of APC-conjugated D^b:$VP2_{121-130}$ tetramer (National Institutes of Health Tetramer Core Facility) was used in a 30-min incubation step in the dark at room temperature. TGFβ RI-PE (dilution: 10μl/test; Cat: FAB5871P), Rat IgG2A-PE (dilution: 10μl/test; IC006P), TGFβ RII-PE (10μl/test; cat: FAB532P) and Goat IgG-PE (dilution: 10μl/test; IC108P; all from R & D Systems) surface staining were performed according to the manufacturer's instruction. For intracellular staining, surface-stained cells were fixed and permeabilized with the FOXP3/Transcription Factor Staining Buffer Set (00-5523-00; eBiosciences), followed by incubation with fluorochrome-conjugated anti- FOXP3-FITC or anti- FOXP3-APC (dilution: 1/200; clone: FJK-16s Cat: 17-5773-82; eBioscience); anti-Helios-Brilliant Violet 421 (dilution: 1/200; clone: 22F6; cat: 137234; BioLegend) or anti-Helios-PerCP/Cyanine5.5 (dilution: 1/200; clone: 22F6; cat: 137230; BioLegend); anti-RORγT-Brilliant Violet 421 (dilution: 1/200; clone: Q31-378; cat: 562894; BD Biosciences) or anti-RORγT-PE (dilution: 1/200; clone: Q31-378; cat: 562607; BD Biosciences); and anti-TCF-1-Alexa Fluor 647 (dilution: 1/300; clone: C63D9; cat: 6709S; Cell Signaling) for 2 h or overnight at 4 °C. Cells were then washed twice with wash/perm buffer.

For detection of phosphorylated signaling proteins (S6 and STAT5), lymphocytes were rested in complete medium for 1 h at 37 °C. They were fixed with Phosflow Lyse/ Fix buffer (558049; BD Biosciences), followed by permeabilization with Phosflow Perm buffer III (558050; BD Biosciences) and were stained with antibody to PE-conjugated S6 phosphorylated at Ser235 and Ser236 (dilution: 1/100; clone: D57.2.2E; cat: 5316S) and rabbit IgG-PE (dilution: 1/200; clone: DA1E; cat: 5742S; both from Cell Signaling Technology), FITC-conjugated STAT5 phosphorylated at Tyr694 (dilution: 1μg/test; clone: SRBCZX; cat: 11-9010-42) and Mouse IgG1 kappa-FITC (dilution: 1μg/test; clone: P3.6.2.8.1; cat: 11-4714-81; both from eBioscience).

For detection of phosphorylated signaling proteins (Smad2/Smad3), lymphocytes were rested in serum free media for 3 h at 37 °C, prior to 15 min stimulation with 10 ng/ml of TGFβI (Peprotech). They were fixed with Phosflow Lyse/ Fix buffer, followed by permeabilization with Phosflow Perm buffer III and were stained with antibody to PE-conjugated Smad2/Smad3 phosphorylated at Ser465/467 and Ser423/425 (dilution: 1/50; clone: D27F4; cat: 11979S) and rabbit IgG-PE (dilution: 1/100; clone: DA1E; cat: 5742S; both from Cell Signaling Technology).

All flow cytometry data were acquired on LSRII or LSR Fortessa X20 (BD Biosciences) and analyzed with Flowjo software (Tree Star).

In vivo T_H1 polarization and intracellular IFNγ staining

Mice were injected *i.p.* with TMEV and euthanized after seven days. Mesenteric lymph nodes and spleen were collected. Single cells suspension was prepared and stimulated with 50 ng/ml phorbol-12-myristate-13-acetate (PMA, P1585; Sigma) and 0.75 μg/ml ionomycin

(13909; Sigma) for 5 h in the presence of 1 μg/ml GolgiStop (555029; BD Biosciences) before intracellular staining. Cells were surface-stained followed by IFNγ (dilution: 1/200; clone: XMG1.2; cat: 17-7311-82; eBioscience) intracellular staining.

In vivo T_H17 polarization and intracellular IL-17A staining

Mice were injected intraperitoneally three times with CD3-specific antibody (20 μg per mouse; 2C11; BioLegend) or PBS at 0, 48 and 96 h, as described earlier[48]. 100 h after the first injection, the small bowel was enzymatically dispersed, intraepithelial cells (IEL) and lamina propria (LP) cells were isolated, and re-stimulated with PMA/Ionomycin and 5 h later were stained for intracellular IL-17A (dilution: 1/300; clone: TC11-18H10; cat: 559502; BD Biosciences).

In vitro T-cell polarization assay

Total $CD4^+$ T-cells from spleen of *Foxp3*^{Cre} and *Foxp3*^{Cre}*Tcf7*$^{fl/fl}$ mice were negatively isolated through the use of a mouse $CD4^+$ T-cell Isolation Kit (130-104-454; Miltenyi). 1×10^5 $CD4^+$ T-cells were seeded with 1×10^5 irradiated antigen presenting cells, 0.75 μg/ml anti-CD3 (2C11; BioLegend) and 1.5 μg/ml anti-CD28 (37.51; BioLegend) in a coated plate. For T_H1 polarization, cells were supplemented with 5 μg/ml of anti-IL-4 (11B11; BD Biosciences), 10 ng/ml of IFNγ (485-MI-100; R & D Systems), and 10 ng/ml of IL-12 (419-ML; R & D Systems). For T_H17 polarization, cells were treated with 5 μg/ml of anti-IL-4, 5 μg/ml of anti-IFNγ (XMG1.2; eBioscience), 10 μg/ml of anti-IL-2 (JES6-5H4; Bio Cell), 30 ng/ml of IL-6 (406-ML; R & D Systems) and 1.5 ng/ml of TGFβI (PHG9204; Thermo Fisher). After 65 h, cells were removed from the TCR signaling and recultured in a non-coated plate. Four days after activation, cells were re-stimulated with PMA/Ionomycin/GolgiStop for 5 h, followed by IFNγ and IL-17A staining.

In other experiments, $CD4^+CD25^-CD62L^{hi}CD44^{lo}$ naïve T-cells were FACS sorted from MACS-pre-purified naïve $CD4^+$ T-cells (130-104-453; Miltenyi) isolated from spleen of WT CD45.1 mouse and labeled with 4 μM Cell Trace Violet (C34557; Thermo Fisher). $CD25^+YFP^+$ CD45.2 Treg cells were FACS sorted from MACS-pre-purified $CD4^+$ T-cells (130-104-454; Miltenyi) isolated from spleen of *Foxp3*^{Cre} and *Foxp3*^{Cre}*Tcf7*$^{fl/fl}$ mice. Cells in equal number were stimulated under T_H1 or T_H17 polarized conditions in presence of irradiated splenocytes at 1:1:3 ratio for 90 h. Cells were cultured in RPMI-1640 with L-glutamine (12-702F; Lonza) with 10% FBS, 0.5 mM L-glutamine (25030-081; Life Technologies), 1 mM Sodium pyruvate (Sigma), 100 IU/ml penicillin and 100 mg/ml streptomycin (15140-122; both from Life Technologies), 50 μM/ml β-mercaptoethanol (M3148; Sigma). All cultures were performed in a volume of 200 μl in 96-well U-bottomed plates.

T-cell proliferation suppression assay

$CD25^+YFP^+$ CD45.2 T_{reg}-cells as suppressor cells were FACS sorted from MACS-pre-purified $CD4^+$ T-cells (130-104-454; Miltenyi) isolated from spleen of *Foxp3*^{Cre} and *Foxp3*^{Cre}*Tcf7*$^{fl/fl}$ mice. $CD4^+CD25^-CD62L^{hi}CD44^{lo}$ naïve T-cells as responder cells were FACS sorted from MACS-pre-purified naïve $CD4^+$ T-cells (130-104-453; Miltenyi) isolated from spleen of WT CD45.1 mouse. T responder cells were labeled with 2.5 μM CFSE and

then cocultured with T_{reg}-cells (30×10^3) at a 1:1 ratio with or without allogeneic $CD11c^+$ cells (120×10^3) for 72 h. Allogeneic DC from Balb/c mice was obtained by incubation with MACS microbeads coated with anti-CD11c mAb (130-104-453; Miltenyi Biotech) and irradiated at 3,000 rad. Cells were activated with anti-CD3 (0.5 μg/ml) by coating 96-well round bottom plates for 2 h at 37 °C.

Histology and immune staining

Gut tissues were harvested, opened longitudinally and fixed using 10% formalin for 12–18 h, and routinely paraffin embedded and processed. For immune staining, 5-μm thick tissue sections were deparaffinized in xylene and rehydrated in ethanol. Following rehydration, slides were immersed in target retrieval solution (S1699; Dako), and heat-induced epitope retrieval was performed in a Decloaking Chamber (Biocare Medical). Following antigen retrieval, tissues were washed with PBS and nonspecific background staining was blocked using dual endogenous enzyme block (S2003; Dako), Fc-block (2.4G2, Antibody Hybridoma Core, Mayo Clinic; kindly provided by Dr Tom Beito), and Background Sniper (BS966L; BioCare Medical). Nonspecific avidin/biotin was blocked when needed (SP-2001; Vector Laboratories). Primary antibodies were diluted in antibody diluent solution (S0809; Dako) and incubated overnight at 4 °C. For β-catenin staining, anti-β-catenin (dilution: 1/200; clone: 14/ β-catenin (RUO); cat: 610154; BD Biosciences) as primary and Envision + System-HRP-labelled polymer anti-mouse (K4001; Dako) as a secondary antibody was used for 45 min. For Gr1 staining, anti-Gr1 (dilution: 1/50; clone: NIMP-R14; cat: NB600-1387; Novus Biologicals) as primary and biotinylated rabbit anti-rat (BA-4001; Vector Laboratories) as secondary antibodies were applied to the sections for 45 min, followed by streptavidin (HRP conjugate, 016-030-084; Jackson Laboratories) for 30 min. Counterstaining was done using Chromogen DAB+Substrate (K3468; Dako) followed by hematoxylin counterstain. A Leica light microscope mounted with a Zeiss Axiocam 503 camera was used for imaging of Immunohistochemistry staining.

mRNA isolation for RNA sequencing

2-4.0 x 10^5 $CD25^+YFP^+$ T_{reg}-cells were FACS sorted from MACS-pre-purified $CD4^+$ T-cells (mouse $CD4^+$ T-cell Isolation Kit, Miltenyi) isolated from MLNs of *Foxp3*^{Cre} and *Foxp3*^{Cre}*Tcf7*$^{fl/fl}$ mice. Total RNA was isolated using the PicoPure RNA Isolation Kit (Arcturus) following the manufacturer's instructions. Libraries were generated and sequenced by the University of Chicago Genomics Facility.

Single cell RNA-Seq

$CD25_+YFP_+$ T_{reg}-cells were FACS sorted from MACS-pre-purified $CD4_+$ T-cells (mouse $CD4_+$ T-cell Isolation Kit, Miltenyi) isolated from MLN of $Foxp3_{Cre}$ and $Foxp3^{Cre}Tcf7^{fl/fl}$ mice and immediately submitted to the Genomics Facility. The cells were first counted and measured for viability using the Vi-Cell XR Cell Viability Analyzer (Beckman-Coulter), as well as a basic hemocytometer with light microscopy. The barcoded Gel Beads were thawed from −80°C and the reverse transcription master mix was prepared according to the manufacturer's instructions for Chromium Single Cell 3' v2 library kit (10x Genomics). Based on the desired number of cells to be captured for each sample, a volume of live cells was mixed with the master mix. The cell suspension/master mix, thawed Gel Beads and

partitioning oil were added to a Chromium Single Cell A chip. The filled chip was loaded into the Chromium Controller, where each sample was processed and the individual cells within the sample were captured into uniquely labeled GEMs (Gel Beads-In-Emulsion). The GEMs were collected from the chip and taken to the bench for reverse transcription, GEM dissolution, and cDNA clean-up. Resulting cDNA was a pool of uniquely barcoded molecules. Single cell libraries were created from the cleaned and measured, pooled cDNA. During library construction, standard Illumina sequencing primers and unique i7 Sample indices were added to each cDNA pool. Each sample was uniquely indexed.

All cDNA pools and resulting libraries were measured using Qubit High Sensitivity assays (Thermo Fisher Scientific), Agilent Bioanalyzer High Sensitivity chips (Agilent) and Kapa DNA Quantification reagents (Kapa Biosystems).

Libraries were sequenced at 50,000 fragment reads per cell following Illumina's standard protocol using the Illumina cBot and HiSeq 3000/4000 PE Cluster Kit. The flow cells were sequenced as 100 X 2 paired end reads on an Illumina HiSeq 4000 using HiSeq 3000/4000 sequencing kit and HCS v3.3.52 collection software. Base-calling was performed using Illumina's RTA version 2.7.3.

Single cell RNA-Seq data analysis

The 10x Genomics Cellranger (v2.0.2) mkfastq was applied to demultiplex the Illumina BCL output into FASTQ files. Cellranger count was then applied to each FASTQ file to align reads to mm10 reference genome and generate barcode and UMI counts. We followed the Seurat [56] (v3.2.2) integrated analysis and comparative analysis workflows to do all scRNA-Seq analyses [56]. Genes expressed in < 3 cells and cells with < 200 genes or > 15% mitochondrial genes were excluded for downstream analysis in each dataset. Cell cycle score for each cell was calculated by CellCycleScoring function from Seurat using mouse cell cycle genes. SCTransform function was invoked to normalize the dataset (using default parameters), regress out mitochondrial (percent.MT) and cell cycle (S and G2M) contents and identify variable genes.

The datasets were integrated based on "anchors" identified between datasets (nfeatures = 2000, normalization.method = "SCT") prior to performing linear dimensional reduction by Principal Component Analysis (PCA). The top 25 PCs were included in a Uniform Manifold Approximation and Projection (UMAP) dimensionality reduction. Clusters were identified on a shared nearest neighbor (SNN) graph the top 25 PCs with the Louvain algorithm. Differential gene expression was determined by "findMarkers" function with the default Wilcox Rank Sum test either as one versus rest or as a direct comparison with parameters min.pct = 0.1 and logfc.threshold = 0. For Metascape analysis [57], the 200 upregulated genes were then determined based on reported adjusted p-values. For GSEA analysis, a pre-ranked gene list was created based on sorted scores defined by $-\log_{10}$(reported p-value) ×sign(reported average logfc). The cell annotation was based on the top differentially expressed genes.

Gene list module scores were calculated with Seurat function AddModuleScore [58]. This calculates the average scaled expression levels of each gene list, subtracted by the expression

of control feature sets. To compare the single marker expression between cell types, wilcox-test was used.

To calculate the RNA velocity, the loom files were generated from the bam files by Velocyto [40]; The RNA velocity was then calculated using the RunVelocity function in Velocyto.R package. The velocity for each sample was shown by show.velocity.on.embedding.cor function in Velocyto.R package.

Quantification and statistical analysis

Except for deep-sequencing data, statistical significance was calculated with GraphPad Prism software. Error bars in graphs indicate standard error of the mean (SEM) and statistical comparisons were done by unpaired Student's t-test. p values of ≤ 0.05 were considered statistically significant.

Extended Data

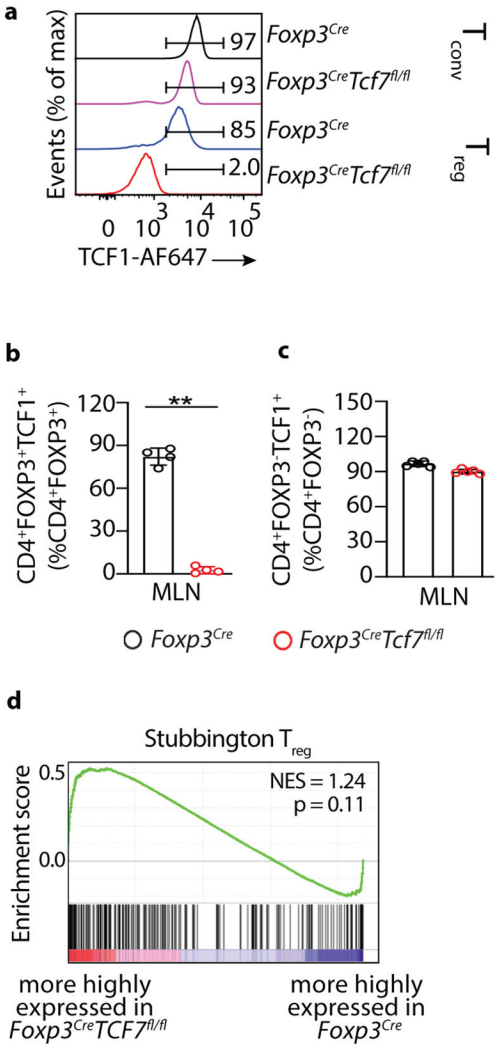

Extended Data Fig 1. TCF-1 deficiency selectively reprograms T_{reg}-cells without compromising their core signature.

T_{reg}-cells were isolated from the mesenteric lymph nodes of *Foxp3*^{Cre} and *Tcf7*$^{fl/fl}$*Foxp3*^{Cre} mice. **(a)** Representative FACS histograms of MLN purified cells from *Foxp3*^{Cre} *Tcf7*$^{fl/fl}$ and control *Foxp3*^{Cre} showing selective loss of TCF-1 from T_{reg}-cells in *Foxp3*^{Cre} *Tcf7*$^{fl/fl}$ mice. (**b** and **c**) Histogram plots showing the cumulative data of the same. (b: $n = 4$; $p < 0.0001$ & c: $n = 5$) Data are representative of two independent experiments and n represents biologically independent replicate mice; means ± SEM; two-sided, unpaired t-test. (**d**) GSEA plot comparing the enrichment of genes expressed more strongly in *Foxp3*^{Cre} versus *Foxp3*^{Cre}*Tcf7*$^{fl/fl}$ T_{reg}-cells.

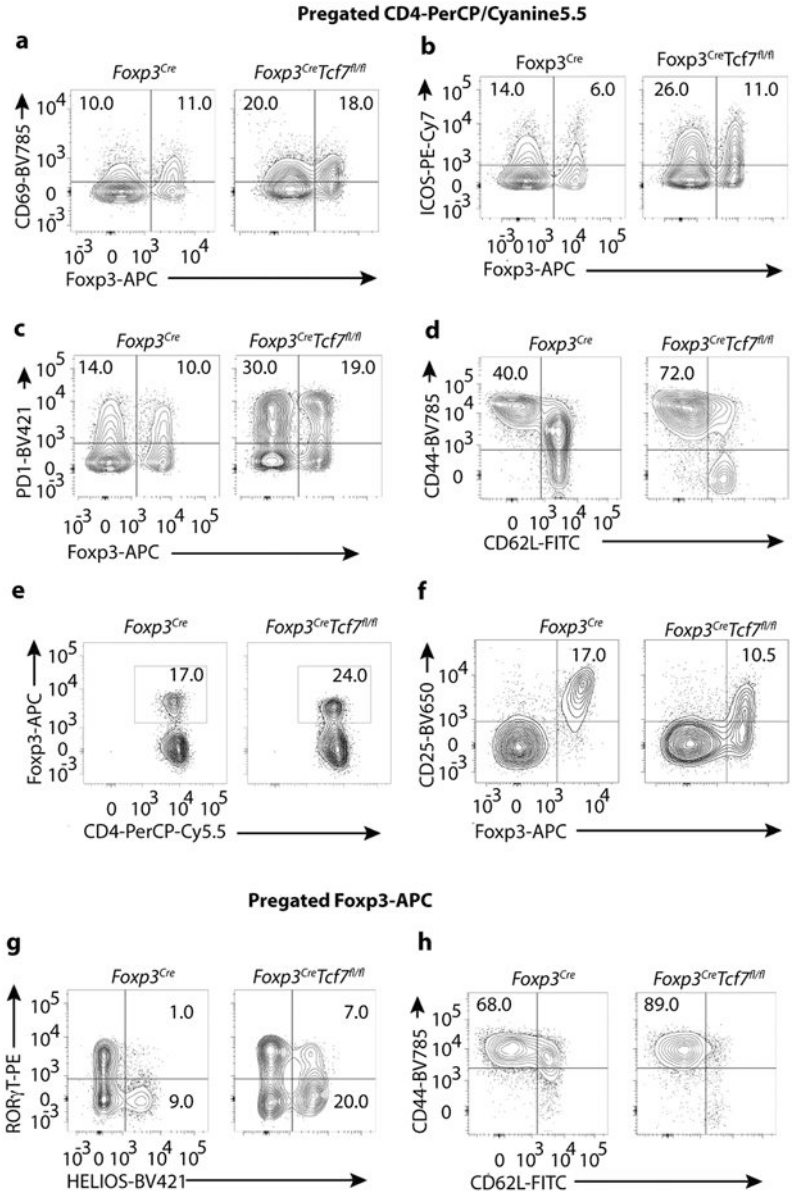

Extended Data Fig. 2. Representative FACS plots of cell lymphocytes surface markers expressed by T_{reg}_cells

T_{reg}-cells were isolated from the mesenteric lymph nodes of *Foxp3*^{Cre} and *Tcf7*$^{fl/fl}$*Foxp3*^{Cre} mice. See cumulative data presented in Figure 2. (a-c) CD4$^+$ cells were pre-gated and frequency of CD69$^+$, ICOS$^+$, and PD1$^+$ cells among CD4$^+$FOXP3$^-$ T_{con} or CD4$^+$FOXP3$^+$ T_{reg}-cells was measured, as indicated. (d) CD4$^+$ cells were pre-gated and frequency of CD44$^+$CD62L$^-$ cells among CD4$^+$FOXP3$^-$ T_{con} cells was measured. (e) CD4$^+$ cells were pre-gated and frequency of CD4$^+$FOXP3$^+$ T_{reg}-cells was measured. (f) CD4$^+$ cells were pre-gated and frequency of FOXP3$^+$CD25$^+$ T_{reg}-cells was measured. (g) CD4$^+$FOXP3$^+$ T_{reg}-cells were pre-gated and frequency of RORγT$^+$HELIOS$^-$ or RORγT$^+$HELIOS$^+$ was measured. (h) CD4$^+$FOXP3$^+$ T_{reg}-cells and frequency of CD44$^+$CD62L$^-$ cells among T_{reg} cells was measured. Numbers inside quadrants indicate percent cells in the respective quadrants.

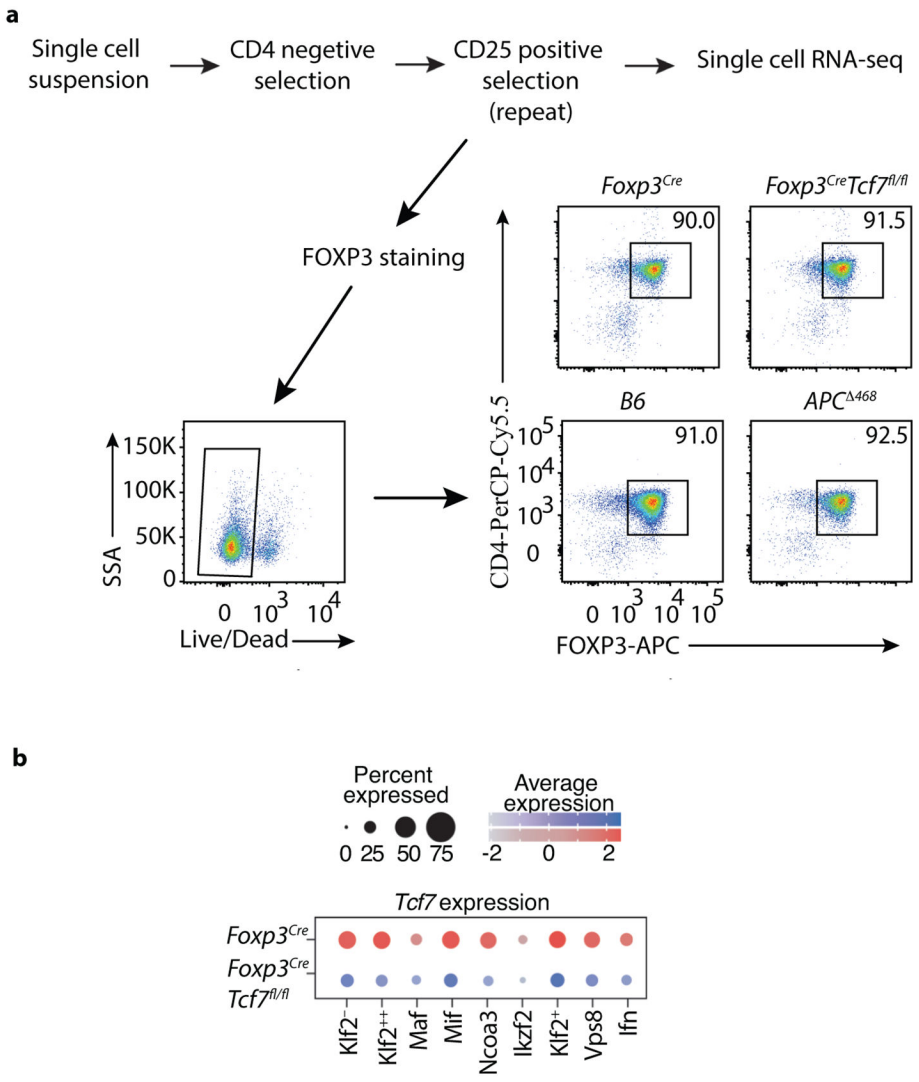

Extended Data Fig. 3. T_{reg} purification.

T_{reg}-cells were isolated from the mesenteric lymph nodes of *Foxp3*^{Cre} and *Tcf7*$^{fl/fl}$*Foxp3*^{Cre} mice. (**a**) Schematic representation of magnetic purification of T_{reg}-cells, and FACS analysis showing over 90% purity. (**b**) Expression changes of the *Tcf7* transcripts between TCF-1-

deficient and TCF-1-sufficient T_{reg}-cells. The color intensity is proportional to the average gene expression across cells in the indicated T_{reg} cluster. The size of circles is proportional to percentage of cells expressing indicated genes.

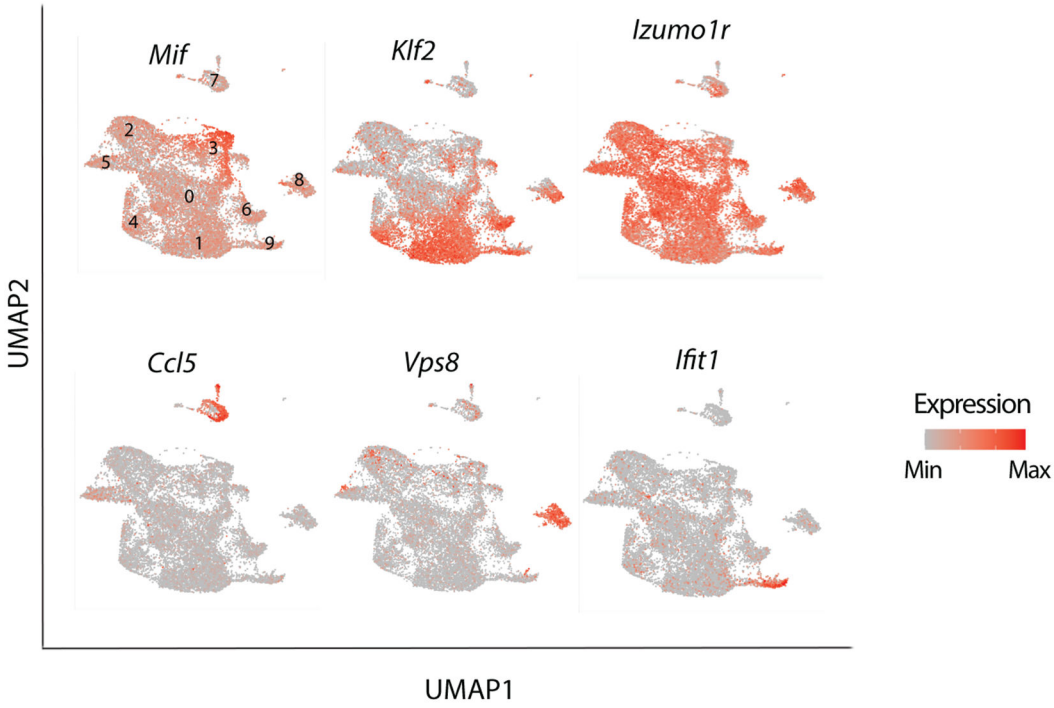

Extended Data Fig. 4. Single-cell RNAseq reveals distinct T_{reg} populations.
mRNA expression of select indicated genes projected on the UMAP. Note varied expression of *Klf2* but broad and uniform expression of *Izumo1r* by T_{reg} clusters, high expression of *Mif,* Vps8, and *Ifit1* in the respective Mif (cluster 3), Vps8 (cluster 8), Ifn (cluster 9). Expression of Ccl5 is prominent in the *Cd63* (cluster 7), which is likely not T_{reg}-cells.

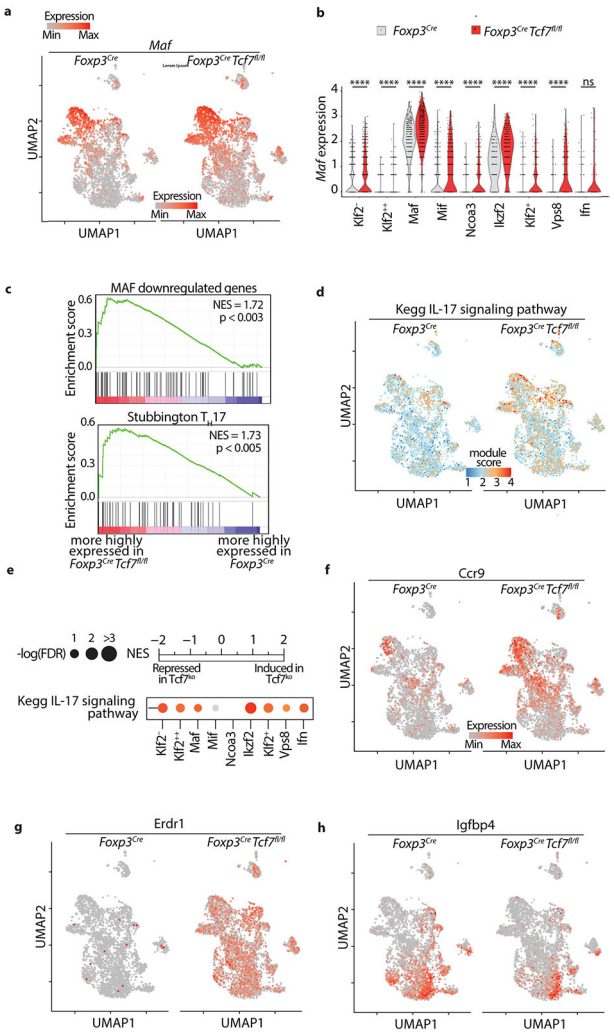

Extended Data Fig. 5. TCF-1-deficient and sufficient T_{reg}-cells show distinct effector functions.

T_{reg}-cells were isolated from the mesenteric lymph nodes of *Foxp3*^{Cre} and *Tcf7*$^{fl/fl}$*Foxp3*^{Cre} mice. (**a**) mRNA expression of *Maf* projected on the UMAP, comparing T_{reg}-cells derived from *Foxp3*^{Cre} to *Tcf7*$^{fl/fl}$ *Foxp3*^{Cre} mice. (**b**) Violin plots showing expression of *Maf* in individual T_{reg} clusters. (**c**) GSEA of MAF downregulated genes and T_H17 pathway defined by Stubbington. (**d**) Kegg IL17 signaling pathway projected on UMAP, comparing TCF-1-sufficient and TCF-1-deficient T_{reg}-cells (**e**) GSEA analysis for the Kegg IL17 signaling pathway comparing transcriptomes of TCF-1-sufficient and TCF-1-deficient T_{reg}-cells across all cell types. Normalized enrichment scores (NES) are color coded. $-\log_{10}$ (FDR) values are proportional to the circle size. FDR>15% are masked with gray color. (**fgh**) mRNA expression of *Ccr9, Erdr1* and *Igfbp4* projected on the UMAP, comparing TCF-1-sufficient and TCF-1-deficient Klf2^{-} cells for the Kegg IL17 pathway.

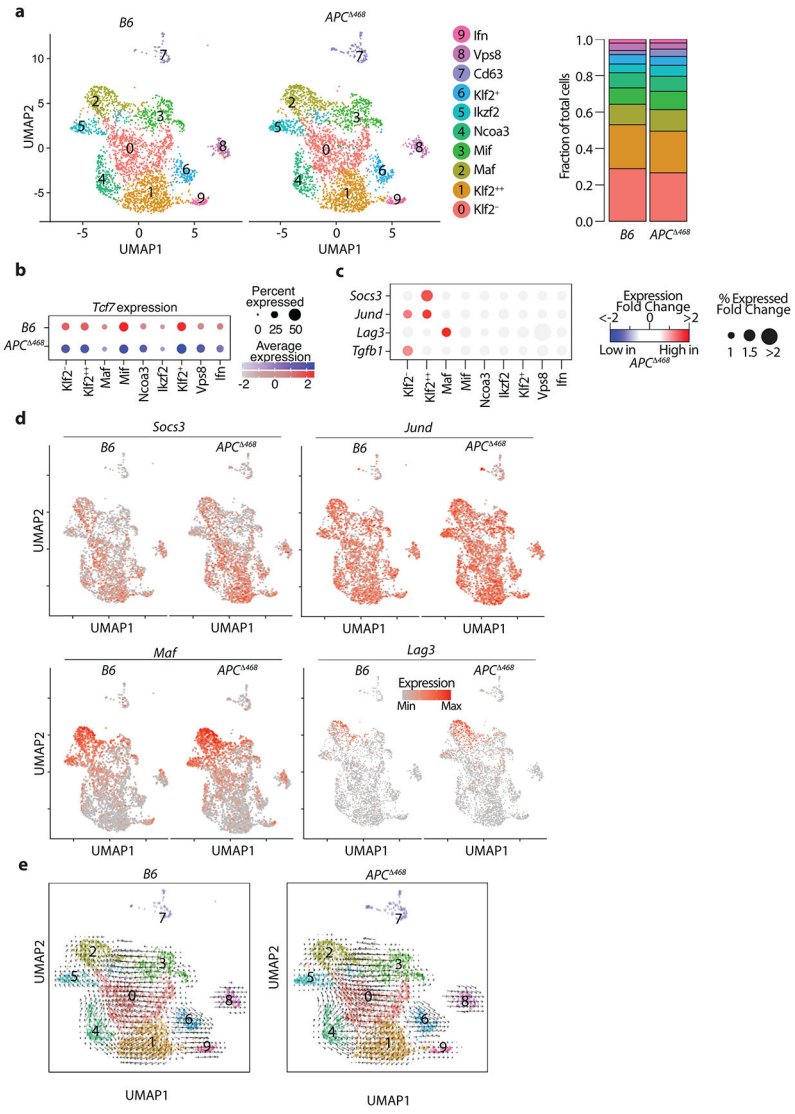

Extended Data Fig. 6. T_{reg}-cells are activated and polarized during polyposis.

T_{reg}_cells were isolated from the mesenteric lymph nodes of WT and *APC*$^{\Delta 486}$ mice. (**a**) UMAP projection (left panel) and fraction of cells in each cell type (stack bars; right panel) for APC$^{\Delta 486}$ and control B6 T_{reg}-cells. Data are from two replicates. (**b**) Dot plot showing the expression of *Tcf7* across all cell types in *Apc*$^{\Delta 486}$ and control *B6* T_{reg}-cells. Color and size of the dots are proportional to the expression level and percent of cells expressing *Tcf7* in each indicated cluster. (**c**) Expression of *Socs3, Jund, Lag3* and *Maf* between *APC*$^{\Delta 486}$ and *B6* cells projected on the UMAP. See TableS4 for the full list. The fold change in percent of cells expressing the indicated gene in each cell type is proportional to the circle size. Adjusted-p-values > 0.01 are masked with gray color. (**d**) Expression changes of the most differentially expressed genes between *APC*$^{\Delta 486}$ and control *B6* T_{reg}_cells. See TableS4 for the full list. The fold change in expression intensities is color-coded. (**e**) RNA velocity vectors overlaid on UMAP for *B6* (left) and *APC*$^{\Delta 486}$ (right) T_{reg}-cells.

Supplementary Material

Refer to Web version on PubMed Central for supplementary material.

Acknowledgments

This work was supported by NIH R01 AI 108682 (FG & KK), NIH RO1 AI 147652 (FG), NIH R35GM138283 (MK), and Praespero Innovation Award Alberta, Canada (FG & KK). Ms Nicoleta Carapanceanu and Mr. Valentin Carapanceanu are thankfully acknowledged for excellent technical support. Dr. Leesaa Pennell (Biolegend) is gratefully acknowledged for advice with single cell RNA sequencing techniques. Ms. Vernadette Simon (Mayo Clinic, Rochester, MN) is gratefully acknowledged for assistance with single cell RNA sequencing. Dr. Alexandra Vitko Lucs (Eli Lilly) is thankfully acknowledged for providing the TGFβRI inhibitor LY3200882 and for scientific advice. We thank Dr. Katrina Woolcock (Lifesciences Editors) for professional editing of the manuscript.

Data Availability

The Bulk and scRNAseq datasets were deposited in the Gene Expression Omnibus (GEO) under the accession code GSE163084. The codes used for bulk and single-cell RNA-seq analysis followed typical pipelines from public R packages (DESeq2 and Seurat). All codes are available upon request.

References

1. Fontenot JD, Gavin MA & Rudensky AY Foxp3 programs the development and function of CD4+CD25+ regulatory T cells. Nat Immunol 4, 330–336 (2003). [PubMed: 12612578]
2. Hori S, Nomura T & Sakaguchi S Control of regulatory T cell development by the transcription factor Foxp3. Science 299, 1057–1061 (2003). [PubMed: 12522256]
3. Khattri R, Cox T, Yasayko SA & Ramsdell F An essential role for Scurfin in CD4+CD25+ T regulatory cells. Nat Immunol 4, 337–342 (2003). [PubMed: 12612581]
4. Benoist C & Mathis D Treg cells, life history, and diversity. Cold Spring Harb Perspect Biol 4, a007021 (2012). [PubMed: 22952391]
5. Ohnmacht Cet al.MUCOSAL IMMUNOLOGY. The microbiota regulates type 2 immunity through RORgammat(+) T cells. Science349, 989–993 (2015). [PubMed: 26160380]
6. Schiering Cet al.The alarmin IL-33 promotes regulatory T-cell function in the intestine. Nature513, 564–568 (2014). [PubMed: 25043027]
7. Pratama A, Schnell A, Mathis D & Benoist C Developmental and cellular age direct conversion of CD4+ T cells into RORγ+ or Helios+ colon Treg cells. J Exp Med 217 (2020).
8. Zhou J, Nefedova Y, Lei A & Gabrilovich D Neutrophils and PMN-MDSC: Their biological role and interaction with stromal cells. Semin Immunol 35, 19–28 (2018). [PubMed: 29254756]
9. Blatner NRet al.Expression of RORgammat marks a pathogenic regulatory T cell subset in human colon cancer. Sci Transl Med4, 164ra159 (2012).
10. Miragaia RJet al.Single-Cell Transcriptomics of Regulatory T Cells Reveals Trajectories of Tissue Adaptation. Immunity50, 493–504 e497 (2019). [PubMed: 30737144]
11. Blatner NRet al.In colorectal cancer mast cells contribute to systemic regulatory T-cell dysfunction. Proc Natl Acad Sci U S A107, 6430–6435 (2010). [PubMed: 20308560]
12. Gounaris Eet al.T-regulatory cells shift from a protective anti-inflammatory to a cancer-promoting proinflammatory phenotype in polyposis. Cancer Res69, 5490–5497 (2009). [PubMed: 19570783]
13. Keerthivasan Set al.beta-Catenin promotes colitis and colon cancer through imprinting of proinflammatory properties in T cells. Sci Transl Med6, 225ra228 (2014).
14. Quandt Jet al.Wnt-beta-catenin activation epigenetically reprograms Treg cells in inflammatory bowel disease and dysplastic progression. Nat Immunol22, 471–484 (2021). [PubMed: 33664518]
15. Sumida Tet al.Activated beta-catenin in Foxp3(+) regulatory T cells links inflammatory environments to autoimmunity. Nat Immunol19, 1391–1402 (2018). [PubMed: 30374130]

16. Mosimann C, Hausmann G & Basler K Beta-catenin hits chromatin: regulation of Wnt target gene activation. Nature reviews. Molecular cell biology 10, 276–286 (2009). [PubMed: 19305417]
17. Barra MM, Richards DM, Hofer AC, Delacher M & Feuerer M Premature expression of Foxp3 in double-negative thymocytes. PLoS One 10, e0127038 (2015). [PubMed: 25978037]
18. Barra MMet al.Transcription Factor 7 Limits Regulatory T Cell Generation in the Thymus. J Immunol195, 3058–3070 (2015). [PubMed: 26324778]
19. van Loosdregt Jet al.Canonical wnt signaling negatively modulates regulatory T cell function. Immunity39, 298–310 (2013). [PubMed: 23954131]
20. Xing Set al.Tcf1 and Lef1 are required for the immunosuppressive function of regulatory T cells. J Exp Med216, 847–866 (2019). [PubMed: 30837262]
21. Mielke LAet al.TCF-1 limits the formation of Tc17 cells via repression of the MAF-RORgammat axis. J Exp Med216, 1682–1699 (2019). [PubMed: 31142588]
22. Emmanuel AOet al.TCF-1 and HEB cooperate to establish the epigenetic and transcription profiles of CD4(+)CD8(+) thymocytes. Nat Immunol19, 1366–1378 (2018). [PubMed: 30420627]
23. Rubtsov YPet al.Regulatory T cell-derived interleukin-10 limits inflammation at environmental interfaces. Immunity28, 546–558 (2008). [PubMed: 18387831]
24. Chapman NM & Chi H mTOR Links Environmental Signals to T Cell Fate Decisions. Front Immunol 5, 686 (2014). [PubMed: 25653651]
25. Neumann Cet al.c-Maf-dependent Treg cell control of intestinal TH17 cells and IgA establishes host-microbiota homeostasis. Nat Immunol20, 471–481 (2019). [PubMed: 30778241]
26. Kim HJet al.Stable inhibitory activity of regulatory T cells requires the transcription factor Helios. Science350, 334–339 (2015). [PubMed: 26472910]
27. Thornton AMet al.Expression of Helios, an Ikaros transcription factor family member, differentiates thymic-derived from peripherally induced Foxp3+ T regulatory cells. J Immunol184, 3433–3441 (2010). [PubMed: 20181882]
28. Fassett MS, Jiang W, D'Alise AM, Mathis D & Benoist C Nuclear receptor Nr4a1 modulates both regulatory T-cell (Treg) differentiation and clonal deletion. Proc Natl Acad Sci U S A 109, 3891–3896 (2012). [PubMed: 22345564]
29. Kovalovsky Det al.Beta-catenin/Tcf determines the outcome of thymic selection in response to alphabetaTCR signaling. J Immunol183, 3873–3884 (2009). [PubMed: 19717519]
30. Pabbisetty SKet al.Peripheral tolerance can be modified by altering KLF2-regulated Treg migration. Proc Natl Acad Sci U S A113, E4662–4670 (2016). [PubMed: 27462110]
31. Beischlag TVet al.Recruitment of the NCoA/SRC-1/p160 family of transcriptional coactivators by the aryl hydrocarbon receptor/aryl hydrocarbon receptor nuclear translocator complex. Mol Cell Biol22, 4319–4333 (2002). [PubMed: 12024042]
32. Zemmour Det al.Single-cell gene expression reveals a landscape of regulatory T cell phenotypes shaped by the TCR. Nat Immunol19, 291–301 (2018). [PubMed: 29434354]
33. Balderhaar HJet al.The CORVET complex promotes tethering and fusion of Rab5/Vps21-positive membranes. Proc Natl Acad Sci U S A110, 3823–3828 (2013). [PubMed: 23417307]
34. Kolinski T, Marek-Trzonkowska N, Trzonkowski P & Siebert J Heat shock proteins (HSPs) in the homeostasis of regulatory T cells (Tregs). Cent Eur J Immunol 41, 317–323 (2016). [PubMed: 27833451]
35. Joller Net al.Treg cells expressing the coinhibitory molecule TIGIT selectively inhibit proinflammatory Th1 and Th17 cell responses. Immunity40, 569–581 (2014). [PubMed: 24745333]
36. Qiu XB, Shao YM, Miao S & Wang L The diversity of the DnaJ/Hsp40 family, the crucial partners for Hsp70 chaperones. Cellular and Molecular Life Sciences CMLS 63, 2560–2570 (2006). [PubMed: 16952052]
37. Weis AM, Soto R & Round JL Commensal regulation of T cell survival through Erdr1. Gut Microbes 9, 458–464 (2018). [PubMed: 29543554]
38. Miyagawa Iet al.Induction of Regulatory T Cells and Its Regulation with Insulin-like Growth Factor/Insulin-like Growth Factor Binding Protein-4 by Human Mesenchymal Stem Cells. J Immunol199, 1616–1625 (2017). [PubMed: 28724578]

39. Bettelli Eet al.Reciprocal developmental pathways for the generation of pathogenic effector TH17 and regulatory T cells. Nature441, 235–238 (2006). [PubMed: 16648838]
40. La Manno Get al.RNA velocity of single cells. Nature560, 494–498 (2018). [PubMed: 30089906]
41. Chen Zet al.Selective regulatory function of Socs3 in the formation of IL-17-secreting T cells. Proc Natl Acad Sci U S A103, 8137–8142 (2006). [PubMed: 16698929]
42. Meixner A, Karreth F, Kenner L & Wagner EF JunD regulates lymphocyte proliferation and T helper cell cytokine expression. Embo j 23, 1325–1335 (2004). [PubMed: 15029240]
43. Woo SRet al.Immune inhibitory molecules LAG-3 and PD-1 synergistically regulate T-cell function to promote tumoral immune escape. Cancer Res72, 917–927 (2012). [PubMed: 22186141]
44. Chen MLet al.Regulatory T cells suppress tumor-specific CD8 T cell cytotoxicity through TGF-beta signals in vivo. Proc Natl Acad Sci U S A102, 419–424 (2005). [PubMed: 15623559]
45. Fahlen Let al.T cells that cannot respond to TGF-beta escape control by CD4(+)CD25(+) regulatory T cells. J Exp Med201, 737–746 (2005). [PubMed: 15753207]
46. Mempel TRet al.Regulatory T cells reversibly suppress cytotoxic T cell function independent of effector differentiation. Immunity25, 129–141 (2006). [PubMed: 16860762]
47. Pavelko KDet al.Theiler's murine encephalomyelitis virus as a vaccine candidate for immunotherapy. PLoS One6, e20217 (2011). [PubMed: 21625449]
48. Esplugues Eet al.Control of TH17 cells occurs in the small intestine. Nature475, 514–518 (2011). [PubMed: 21765430]
49. Gounaris Eet al.Live imaging of cysteine-cathepsin activity reveals dynamics of focal inflammation, angiogenesis, and polyp growth. PLoS One3, e2916 (2008). [PubMed: 18698347]
50. Zhang Yet al.Deep single-cell RNA sequencing data of individual T cells from treatment-naive colorectal cancer patients. Sci Data6, 131 (2019). [PubMed: 31341169]
51. Blatner NR, Gounari F & Khazaie K The two faces of regulatory T cells in cancer. Oncoimmunology 2, e23852 (2013). [PubMed: 23762787]
52. Bos PD & Rudensky AY Treg cells in cancer: a case of multiple personality disorder. Sci Transl Med 4, 164fs144 (2012).
53. Kwon HK, Chen HM, Mathis D & Benoist C Different molecular complexes that mediate transcriptional induction and repression by FoxP3. Nat Immunol 18, 1238–1248 (2017). [PubMed: 28892470]
54. van der Veeken Jet al.The Transcription Factor Foxp3 Shapes Regulatory T Cell Identity by Tuning the Activity of trans-Acting Intermediaries. Immunity53, 971–984.e975 (2020). [PubMed: 33176163]
55. Pavelko KD, Bell MP, Harrington SM & Dong H B7-H1 Influences the Accumulation of Virus-Specific Tissue Resident Memory T Cells in the Central Nervous System. Front Immunol 8, 1532 (2017). [PubMed: 29170671]
56. Butler A, Hoffman P, Smibert P, Papalexi E & Satija R Integrating single-cell transcriptomic data across different conditions, technologies, and species. Nat Biotechnol 36, 411–420 (2018). [PubMed: 29608179]
57. Zhou Yet al.Metascape provides a biologist-oriented resource for the analysis of systems-level datasets. Nat Commun10, 1523 (2019). [PubMed: 30944313]
58. Tirosh Iet al.Dissecting the multicellular ecosystem of metastatic melanoma by single-cell RNA-seq. Science352, 189–196 (2016). [PubMed: 27124452]

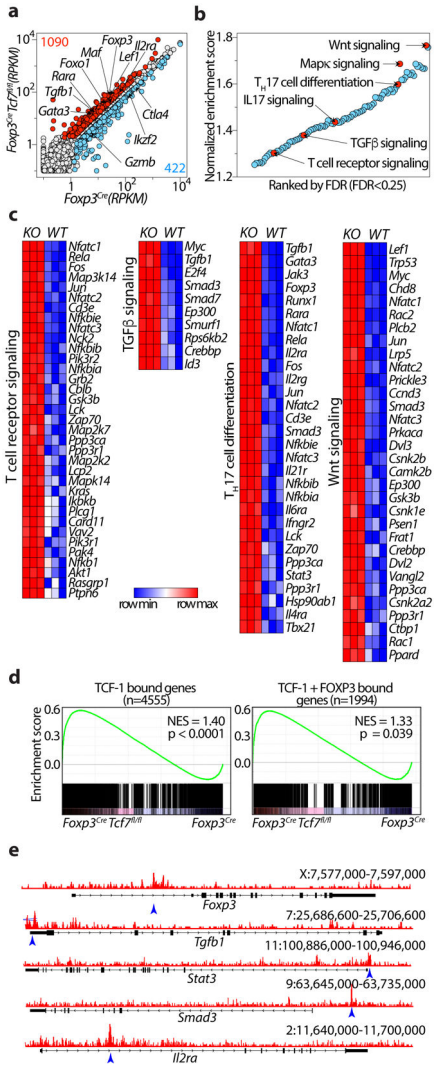

Figure 1: TCF-1 deficiency selectively reprograms T_{reg}-cells without compromising their core signature.

(**a**) Scatter plot comparing the expression of genes in TCF-1-deficient (*Foxp3*^{Cre}*Tcf7*$^{fl/fl}$) and TCF-1-sufficient (*Foxp3*^{Cre}) T_{reg}-cells. Reads Per Kilobase of transcript, per Million mapped reads (RPKM) expression values are average of three biological replicates. Significantly up- or downregulated genes (fold change >1.5 and FDR < 0.001) are shown in red or blue with exact numbers shown at the top or bottom corner, respectively. (**b**) Significantly enriched Kegg pathways by gene set enrichment analysis (GSEA) induced in transcriptomes of TCF-1-deficient versus sufficient T_{reg}-cells. Normalized enrichment scores of all enriched Kegg pathways (FDR< 25%) are shown. Select pathways are highlighted. See TableS1 for the full list. (**c**) The expression of all leading-edge genes from four indicated pathways. See TableS1 for the raw expression levels of all genes. (**d**) GSEA plots showing the enrichment of genes expressed more highly in TCF-1-deficient (*Tcf7*$^{fl/fl}$ *Foxp3*^{Cre}) versus TCF-1-sufficient (*Foxp3*^{Cre}) T_{reg}-cells for genes that are bound by TCF-1 (upper panel) or co-bound by TCF-1 and FOXP3 (lower panel). (**e**) TCF-1 ChIP-seq tracks in mouse T_{reg}-cells showing the *Foxp3, Tgfb1, Stat3, Smad3* and *Il2ra* gene loci. For

simplicity, the input control signal is subtracted from visualized tracks using IGV tools. Detected TCF-1 bound sites against the input control are indicated with blue arrow. Data in **d-e** are from GSE139960.

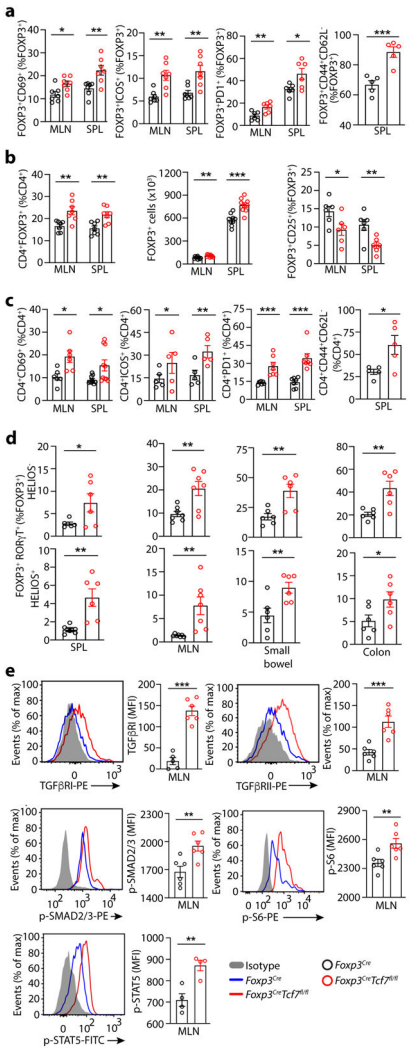

Figure 2: Cumulative data from FACS analysis shows activation and expansion of T_{reg}-cells and $CD4^+$ T_{conv}-cells in TCF-1 deficient mice.

T_{reg}-cells and $CD4^+$ T_{eff}-cells from 5.5-month-old *Foxp3*^{Cre}*Tcf7*$^{fl/fl}$ mice and control *Foxp3*^{Cre} mice were analyzed by FACS. **(a)** Frequency of $CD4^+Foxp3^+$ T_{reg}-cells expressing CD69 (MLN: $n = 7$, $p < 0.01$ & SPL: $n = 7$, $p < 0.006$), ICOS (MLN: $n = 7$, $p < 0.002$ & SPL: $n = 7$, $p < 0.004$), PD-1 (MLN: $n = 6$, $p < 0.006$ & SPL: $n = 6$, $p < 0.02$), and CD44 and CD62L (SPL: $n = 5$, $p < 0.001$) **(b)** Frequencies of T_{reg}-cells (MLN: $n = 7$, $p < 0.005$ & SPL: $n = 7$, $p < 0.004$), and absolute numbers of T_{reg}-cells (MLN: $n = 9$, $p < 0.003$ & SPL: $n = 7$, $p < 0.0002$), and their expression of CD25 (MLN: $n = 6$, $p < 0.03$ & SPL: $n = 6$, $p < 0.009$). **(c)** Frequencies of conventional $CD4^+$ T-cells expressing CD69 (MLN: $n = 6$, $p < 0.01$ & SPL: $n = 10$, $p < 0.01$), PD-1 (MLN: $n = 7$, $p < 0.0008$ & SPL: $n = 7$, $p < 0.0004$), ICOS(MLN: $n = 6$, $p < 0.01$ & SPL: $n = 6$, $p < 0.002$), and CD44 and CD62L (SPL: $n = 5$, $p < 0.02$). **(d)** The frequencies of $HELIOS^-$ or $HELIOS^+FOXP3^+ROR\gamma T^+$ T_{reg}-cells, in the spleen ($n = 6$, $p < 0.04$ or $p < 0.004$), MLN ($n = 7$, $p < 0.005$), small bowel ($n = 6$, $p < 0.006$ or $p < 0.01$), and colon ($n = 6$, $p < 0.006$ or $p < 0.04$). **(a, b, c & d)** Data are representative of two or more independent experiments**. (e)** Representative FACS histograms

normalized to mode (left) and bar diagrams of cumulative data for expression of TGFβRI (n = 6, p < 0.0001), TGFβRII (n = 6, p < 0.0008), p-SMAD2/3 (n = 6, p < 0.006), p-S6 (n = 6, p < 0.009), and p-STAT5 (n = 5, p < 0.005) by T_{reg}-cells. Data are representative of three independent experiments. In all experiments n represents biologically independent animals; means ± SEM, two-sided unpaired t-test.

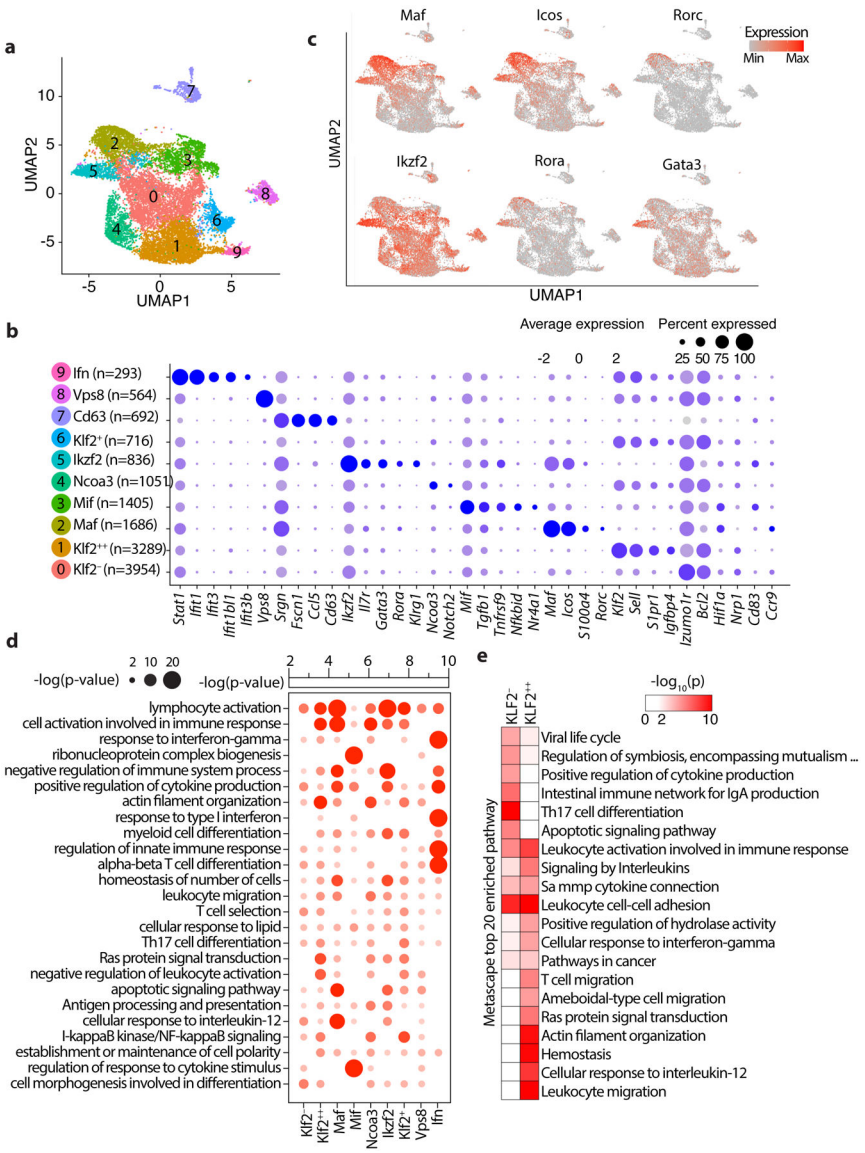

Figure 3: Single cell transcriptomics delineates distinct T_{reg} subpopulations in the mesenteric lymph nodes.

(**a**) Integrated UMAP showing 10 major T_{reg} cell types isolated from the MLNs of mice used in this study. (**b**) Expression of cell-defining features across all cell types. Color intensity is proportional to the average of gene expression across cells in the indicated clusters. The size of circles is proportional to percentage of cells expressing indicated genes. (**c**) mRNA expression of select indicated genes projected on the UMAP, focusing on features of the Maf and Ikzf2 T_{reg} clusters. (**d**) Significantly enriched pathways by Metascape based on top 200 genes upregulated in indicated cell type compared to all other cell types. See TableS2 for the full list. (**e**) 20 most significantly enriched pathways by Metascape based on genes upregulated in $Klf2^{-}$ or $Klf2^{++}$ cell types compared directly to $Klf2^{++}$ or $Klf2^{-}$ cell types, respectively.

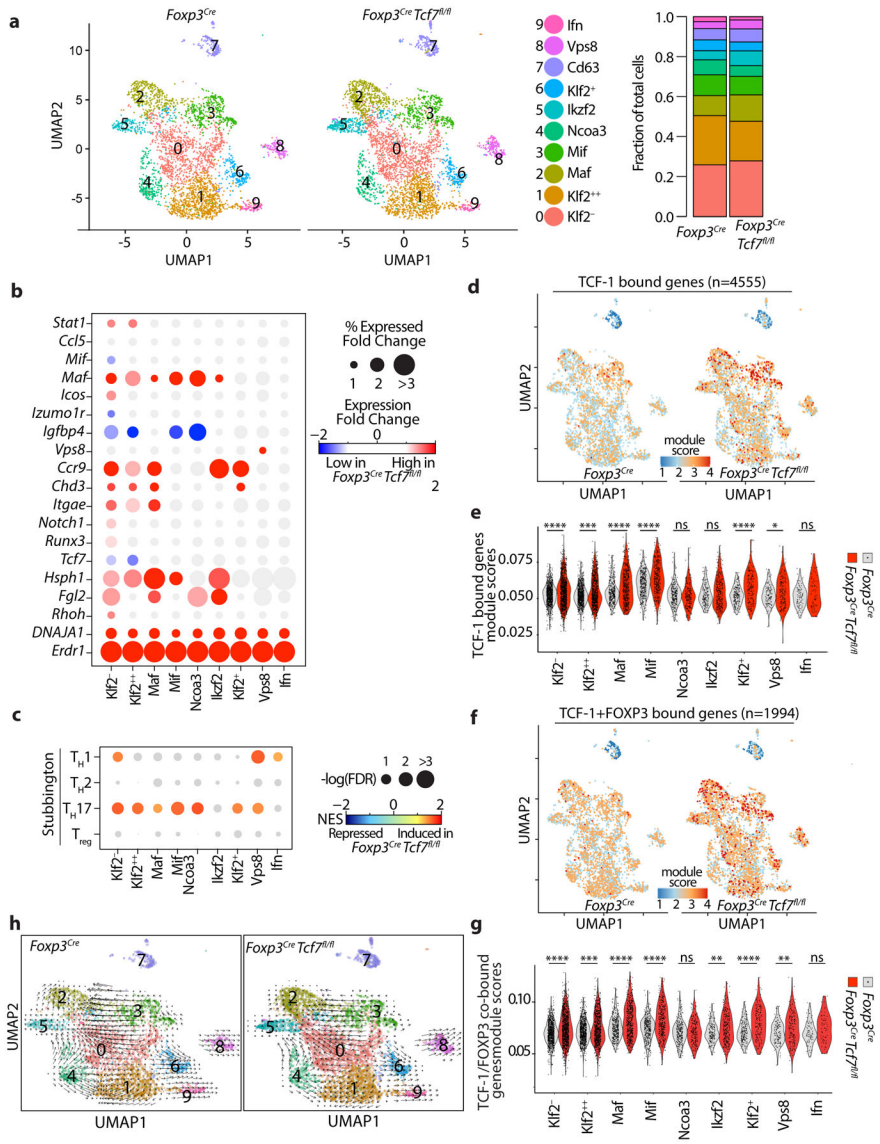

Figure 4: TCF-1-deficient and sufficient T_{reg}-cells show distinct effector functions.

(**a**) UMAP projection (left) and fraction of cells in each cell type (stackbars; right panel) for TCF-1-sufficient (*Foxp3*^{Cre}) and TCF-1-deficient (*Foxp3*^{Cre}*Tcf7*$^{fl/fl}$) T_{reg}-cells. Data are from two replicates. (**b**) Expression changes of the most differentially expressed genes between TCF-1-deficient and sufficient T_{reg}-cells. See TableS3 for the full list. The fold change in expression intensities is color-coded. The fold change in percent of cells expressing the indicated gene in each cell type is proportional to the circle size. (**c**) GSEA analysis for the indicated gene lists comparing transcriptomes of TCF-1-sufficient and TCF-1-deficient T_{reg}-cells across all cell types. Normalized enrichment scores (NES) are color coded. $-\log_{10}$ (FDR) values are proportional to the circle size. FDR>15% are masked with gray color. (**d**) The UMAP projection of module scores for relative expression of TCF-1 bound genes, (**e**) related violin plots. (**f**) The UMAP projection of module scores for relative expression of TCF-1 and FOXP3 co-bound genes, (**g**) related violin plots. (**h**) UMAP and extrapolated future state of cells (overlaid arrows) based on RNA velocity for

TCF-1-sufficient (*Foxp3*^{Cre}) and TCF-1-deficient (*Foxp3*^{Cre} *Tcf7*$^{fl/fl}$) T_{reg}-cells. * $p < 0.05$, *** $p < 0.001$, **** $p<0.0001$ by one-sided (e) or two-sided(g) Wilcoxon test.

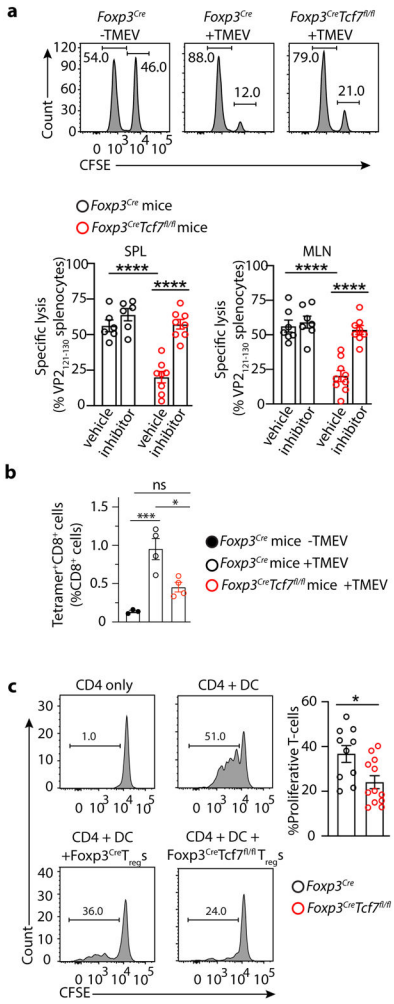

Figure 5: TCF-1-deficient T_{reg}-cells suppress viral antigen specific $CD8^+$ T-cell cytotoxicity and T-cell proliferation.

Foxp3^{Cre} *Tcf7*$^{fl/fl}$ and control *Foxp3*^{Cre} mice at 7-8 weeks of age were compared for their anti-viral T-cell response. **(a)** Representative FACS histograms and cumulative data of viral antigen specific lysis of $VP2_{121-130}$ specific pulsed splenocytes after adoptive transfer in the indicated mice. An equal mix of TMEV-$VP2_{121-130}$ peptide pulsed and unpulsed splenocytes were labelled with different concentrations of CFSE and adoptive transferred to the indicated mice seven days after infection of the mice with TMEV at the peak of response to viral infection. Antigen specific lysis of the splenotyces was measured in the MLN (*Foxp3*^{Cre}: $n = 6$, not significant; *Foxp3*^{Cre} *Tcf7*$^{fl/fl}$: $n = 8$, $p < 0.0001$) and spleen (*Foxp3*^{Cre}: $n = 6$, not significant; *Foxp3*^{Cre} *Tcf7*$^{fl/fl}$: $n = 8$, $p < 0.0001$), four hours after transfer, and calculated after normalizing for nonspecific death of splenocytes transferred in naïve uninfected mice. Data are representative of two or more independent experiments. To block T_{reg} suppression of CD8 T-cells, we treated a separate set of mice from the day of infection with a small molecule inhibitor of TGFβR1 (LY3200882, Eli Lilly), and compared with vehicle control. **(b)** Cumulative data of tetramer FACS analysis of $VP2_{121-130}$ specific $CD8^+$ T-cells in the spleen (*Foxp3*^{Cre} −TMEV: $n = 3$, $p < 0.003$ & $p < 0.007$; *Foxp3*^{Cre} +TMEV: $n = 4$, $p < 0.01$; *Foxp3*^{Cre} *Tcf7*$^{fl/fl}$ +TMEV: $n = 4$) of mice at the peak of response

to TMEV, on day 7 post viral infection. **(c)** Representative FACS histograms and cumulative data of T_{reg} inhibition of $CD4^+$ T-cell proliferation. Percent of proliferating cells in the *in vitro* assays are shown. FACS sorted $CD4^+CD25^-$ cells from the spleen of C57B/6 mice were labelled with CFSE and incubated alone or with irradiated allogenic BALB/c dendritic cells (DC) and αCD3, with or without equal numbers of purified T_{reg}-cells from the indicated mice. Dilution of CFSE by CD4 gated cells was measure after 3 days. Data are representative of three independent experiments with (*Foxp3*^{Cre}: n =5 & *Foxp3*^{Cre} *Tcf7*$^{fl/fl}$: n = 6; $p < 0.01$). In all experiments n represents biologically independent animals; means ± SEM, two-sided, unpaired t-test.

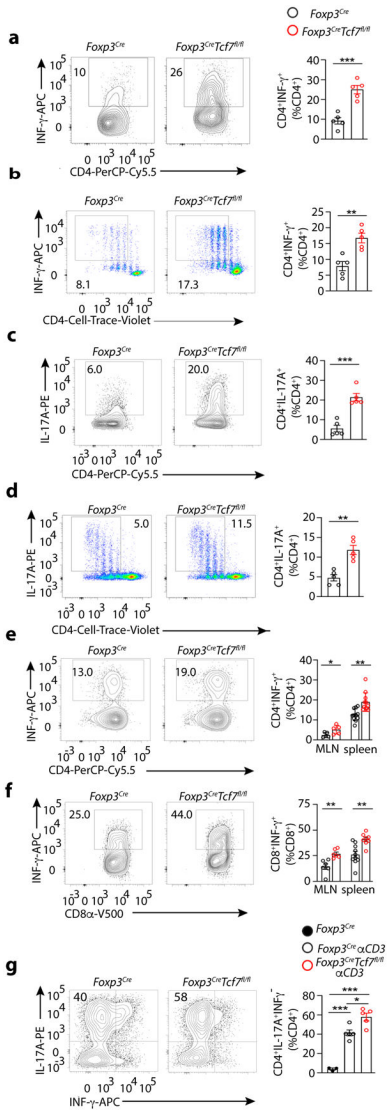

Figure 6: TCF-1-deficient T_{reg}-cells fail to suppress T_H1 or T_H17 polarization of $CD4^+$ T_{conv} cells.

Foxp3^{Cre} *Tcf7*$^{fl/fl}$ and control *Foxp3*^{Cre} mice at 5 months of age were assayed for efficiency of CD4 T-cell polarization, using *in vitro* and *in vivo* assays. Representative FACS contour-plots (left) and cumulative histogram plots (right) are shown. **(a)** T_H1 polarization *in vitro*, using total $CD4^+$ splenocytes from the indicated mice. Magnetically purified $CD4^+$ splenocytes containing both T_{conv} and T_{reg}-cells from the indicated mice were stimulated *in vitro* under T_H1 polarization conditions for 4 days and stained for CD4 and intracellular IFNγ ($n = 5$, $p < 0.0004$). **(b)** T_H1 polarization *in vitro*, with equal numbers of $CD4^+$ T_{reg}-cells and $CD4^+$ T_{conv} cells of the indicated mice. FACS purified $CD62L^+CD44^-CD25^-CD45.1^+CD4^+$ cells from spleen were labelled with Cell Trace Violet, mixed 1:1 with $YFP^+CD45.2^+CD4^+CD25^+$ spleen T_{reg}-cells, and stimulated under T_H1 polarization conditions and assayed by FACS. IFNγ expression gated on $CD45.1^+$ cells ($n = 5$, $p < 0.002$). **(c)** T_H17 polarization *in vitro*, using total $CD4^+$ splenocytes from the indicated mice. $CD4^+$ splenocytes were purified and assayed as in “a”, and were stained

for CD4 and intracellular IL-17A ($n = 5$, $p < 0.0003$; means ± SEM; two-sided, unpaired t-test). **(d)** T_H17 polarization *in vitro*, with equal numbers of T_{reg}-cells and $CD4^+$ T_{conv} cells of the indicated mice. Cells were purified and mixed and analyzed by FACS as in "b", for expression of intracellular IL-17A ($n = 5$, $p < 0.001$). **(e)** Quantitation of *in vivo* T_H1 response to infection with TMEV. The indicated mice were assessed by FACS on day 7 post infection for expression of IFNγ by MLN ($n = 5$, $p < 0.04$) and spleen ($n = 11$, $p < 0.001$) derived $CD4^+$ T-cells. **(f)** The same for $CD8^+$ T-cells (MLN: $n = 4$, $p < 0.04$; spleen: *Foxp3*^{Cre}: $n = 6$ & *Foxp3*^{Cre} *Tcf7*$^{fl/fl}$: $n = 4$; $p < 0.003$). **(g)** Quantitation of *in vivo* T_H17 response after IP injection of αCD3. The indicated mice were assessed by FACS after 3 consecutive injections with antibody (see Materials and Methods) for expression of IL-17A by small bowel residing $CD4^+$ T-cells (*Foxp3*^{Cre}: $n = 3$, $p < 0.0001$; *Foxp3*^{Cre} αCD3: $n = 5$; $p < 0.01$; *Foxp3*^{Cre} *Tcf7*$^{fl/fl}$ αCD3: $n = 5$). Data are representative of two or more independent experiments. In all experiments *n* represents biological replicates, independent animals; means ± SEM, two-sided, unpaired t-test)

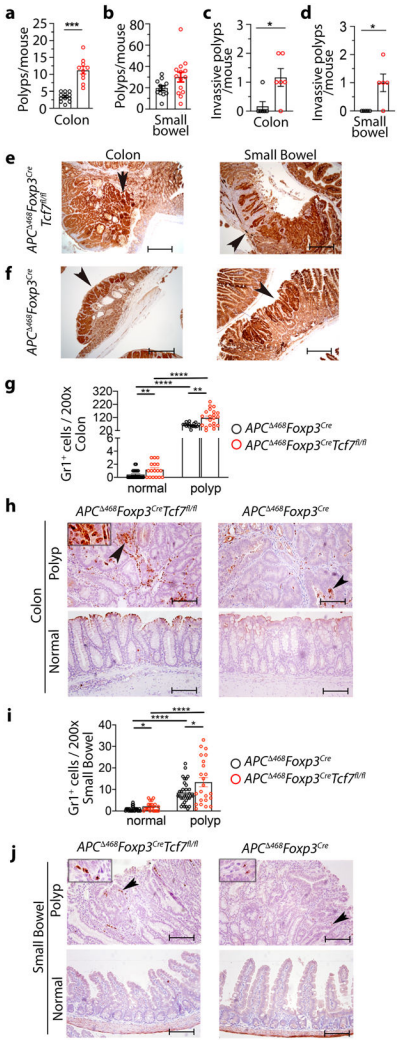

Figure 7. TCF-1-deficient T_{reg}-cells promote inflammation and tumor growth in polyposis-prone *APC*$^{\Delta 468}$ mice.

Tumor incidence, tumor aggression, and inflammation were quantified at 5.5 months of age in *APC*$^{\Delta 468}$*Foxp3*^{Cre}*Tcf7*$^{fl/fl}$ mice and compared to control *APC*$^{\Delta 468}$*Foxp3*^{Cre} mice. **(a and b)** Polyps and tumors in the excised colon (*APC*$^{\Delta 468}$*Foxp3*^{Cre}: $n = 12$ & *APC*$^{\Delta 468}$*Foxp3*^{Cre}*Tcf7*$^{fl/fl}$: $n = 10$; $p < 0.0001$) and small bowel (*APC*$^{\Delta 468}$*Foxp3*^{Cre}: $n = 12$ & *APC*$^{\Delta 468}$*Foxp3*^{Cre}*Tcf7*$^{fl/fl}$: $n = 14$; not significant) were visualized using a dissection microscope and manually counted. **(c and d)** Invasive lesions in the colon ($n = 6$; $p < 0.01$) and the small bowel ($n = 5$; $p < 0.02$). For the cumulative data (a, b, c & d), each symbol represents a value from an individual mouse. Tumor aggression was evaluated by counting lesions that had extensive nuclear β-catenin staining at the submucosal boundary, as determined by IHC. Benign polyps were identified by restricted β-catenin staining at the luminal boundary of the lesions. Each symbol represents a value from an individual mouse. **(e and f)** Representative IHC of colon and small bowel for nuclear β-catenin; scale bar 200 μm. **(g and h)** Quantification of Gr1 stained cells in the colon and representative IHC stained sections; scale bar 100 μm. **(i and j)** Quantification of Gr1 stained cells in the small bowel and representative IHC stained sections. Arrows in “h” and “j” point to Gr1

expressing cells. Each symbol represents counts in one field of vision (FOV) at 200x (g: normal: $n = 4$, $p < 0.009$, $p < 0.0001$, and polyp: $n = 4$, $p < 0.001$ & i: normal: $n = 4$, $p < 0.01$, $p < 0.0001$, and polyp: $n = 4$, $p < 0.02$). In all experiments n represents biologically independent animals; means ± SEM; two-sided, unpaired t-test.

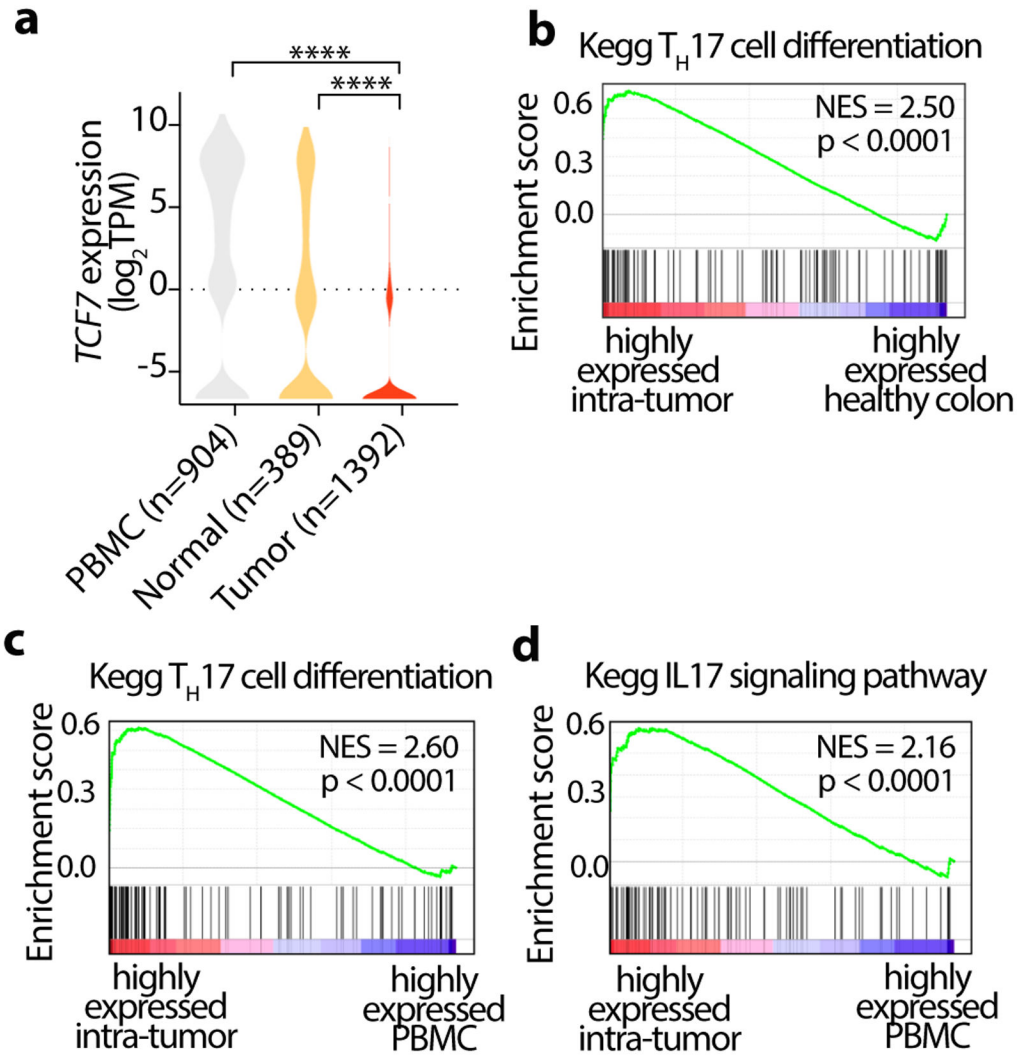

Figure 8. ***Tcf-7*** **is downregulated in CRC tumor-infiltrating T_{reg}-cells.**

Publicly available scRNA-seq data from 12 CRC patients was analyzed, focusing on the T_{reg}-cells from paired peripheral blood mononuclear cells (PBMC), tumor, and adjacent normal tissues. **(a)** Violin plots showing the expression of *Tcf7* in T_{reg}-cells from peripheral blood (PBMC), adjacent normal and tumor tissues. Data is sourced from GSE108989. Number of T_{reg}-cells in each group is indicated in parenthesis. **** p<0.0001 by one-way ANOVA test. (**b-d**) GSEA plots showing highly expressed genes in T_{reg}-cells, (**b**) comparing T_H17 cell differentiation genes in tumor infiltrating to healthy tissue infiltrating T_{reg}-cells, (**c**) comparing T_H17 cell differentiation genes in tumor infiltrating to PBMC T_{reg}-cells (**d**) comparing IL-17 signaling pathway in tumor infiltrating to PBMC T_{reg}-cells, as designated. NES: Normalized enrichment scores.